Coastal REsearch And Transportation Education
Tier 1 University Transportation Center
U.S. Department of Transportation

Dual-Function Near-Surface Mounted Titanium Alloy Bars for Structural Strengthening and Cathodic Protection of Reinforced Concrete Infrastructure
February 11, 2026

(1) Christopher Higgins, Ph.D., P.E., Professor, Oregon State University, School of Civil and Construction Engineering; ORCID: https://orcid.org/0000-0002-2853-3648;Email:chris.higgins@oregonstate.edu

(2) O. Burkan Isgor, Ph.D., Professor, Oregon State University, School of Civil and Construction Engineering; ORCID: https://orcid.org/0000-0002-0554-3501;Email:burkan.isgor@oregonstate.edu

(3) Amanda Slawinski, Former Graduate Student, Oregon State University, School of Civil and Construction Engineering; Email: akslawinski@gmail.com

Final Research Report
Prepared for:
Coastal REsearch And Transportation Education

Technical Report Documentation Form

1. Report No.	2. Government Accession No.	3. Recipient's Catalog No.
2301-9	01895253	n/a

4. Title and Subtitle

Dual-Function Near-Surface Mounted Titanium Alloy Bars for Structural Strengthening and Cathodic Protection of Reinforced Concrete Infrastructure

5. Report Date

02/11/2026

6. Performing Organization Code

n/a

7. Author(s)

(1)Christopher Higgins, Ph.D., P.E., Professor, Oregon State University, School of Civil and Construction Engineering; ORCID: https://orcid.org/0000-0002-2853-364 O 8;Email:chris.higgins@oregonstate.edu

8. Performing Organization Report No.

n/a

9. Performing Organization Name and Address

Oregon State University School of Civil Engineering ,5101 Kearney Hall Corvallis, OR United States 97331-2302

10. Work Unit No. (TRAIS)

n/a

11. Contract or Grant No.

69A3552348330

12. Sponsoring Agency Name and Address

Office of the Assistant Secretary for Research and Technology
University Transportation Centers Program
Department of Transportation
Washington, DC United States 20590

13. Type of Report and Period Covered

Final Project Report
(Full Date)
9/1/2023- 6/01/2026

14. Sponsoring Agency Code

OST-R

15. Supplementary Notes https://create.engineering.txst.edu/

https://create.engineering.txst.edu/

16. Abstract

Corrosion-induced deterioration of reinforced concrete (RC) transportation infrastructure frequently necessitates rehabilitation to address both structural capacity deficiencies and ongoing reinforcement corrosion. These challenges are typically treated independently, with structural strengthening systems restoring capacity and impressed current cathodic protection (ICCP) systems used to mitigate corrosion. This separation increases construction complexity and limits the long-term efficiency of rehabilitation efforts.

This research develops and validates a dual-function rehabilitation system that integrates structural strengthening and corrosion protection into a single near-surface mounted retrofit (NSMR) solution. The system employs high-strength titanium alloy bars (TiABs) as near-surface mounted reinforcement while simultaneously using those bars as ICCP anodes to protect embedded steel reinforcement. A key enabling component is a specially developed electrically conductive structural grout (ECSG) that provides both mechanical bond and electrical connectivity between the TiABs, concrete substrate, and protected reinforcement.

The research program combines electrochemical and structural performance evaluations. Electrochemical testing, including material characterization, small-scale prism experiments, and large-scale beam specimens subjected to active corrosion, demonstrated that TiABs installed with ECSG function effectively as ICCP anodes, achieving stable operating currents, predictable polarization behavior, and compliance with accepted cathodic protection performance criteria. Structural tests included bond (pullout) experiments and large-scale flexural and shear beam tests of specimens representative of vintage RC bridge construction practices. Results confirmed that ECSG-bonded TiABs satisfy development length requirements, restore flexural and shear capacity, and maintain predictable failure modes consistent with established NSMR design practices.

Collectively, the results demonstrate that near-surface mounted TiABs can be deployed as a true dual-purpose system, simultaneously restoring structural capacity and enabling long-term corrosion protection. This report synthesizes the findings into a system-level assessment and provides a foundation for future development and implementation of integrated strengthening and preservation strategies for aging transportation infrastructure.

17. Key Words	18. Distribution Statement
reinforced concrete; corrosion; cathodic protection; near-surface mounted reinforcement; titanium alloy bars; infrastructure rehabilitation	No Restrictions

19. Security Classification (of this report)	20. Security Classification (of this page)	21. No. of Pages	22. Price
Unclassified	Unclassified	63	n/a

Form **DOT F 1700.7** (8-72) **Reproduction of completed page authorized**

ACKNOWLEDGMENT

This study was funded, partially or entirely, by the U.S. Department of Transportation through the Coastal REsearch and Transportation Education University Transportation Center under Grant Award Number 69A3552348330. The work was conducted at Oregon State University. The authors thank project advisory members Jill Atkins of The Perryman Company, Houston, PA and David Andreotti of De Nora Tech, Concord, OH, USA for their guidance and contributions to the development of the dual-functionality components of the reported system. Any opinions, findings, and conclusions or recommendations expressed are those of the authors and do not necessarily reflect the views of the individuals, companies, or federal agencies.

DISCLAIMER

Table of Contents

List of Figures

List of Tables

ABSTRACT

Corrosion-induced deterioration of reinforced concrete (RC) transportation infrastructure frequently necessitates rehabilitation to address both structural capacity deficiencies and ongoing reinforcement corrosion. These challenges are typically treated independently, with structural strengthening systems restoring capacity and impressed current cathodic protection (ICCP) systems used to mitigate corrosion. This separation increases construction complexity and limits the long-term efficiency of rehabilitation efforts.

This research develops and validates a dual-function rehabilitation system that integrates structural strengthening and corrosion protection into a single near-surface mounted retrofit (NSMR) solution. The system employs high-strength titanium alloy bars (TiABs) as near-surface mounted reinforcement while simultaneously using those bars as ICCP anodes to protect embedded steel reinforcement. A key enabling component is a specially developed electrically conductive structural grout (ECSG) that provides both mechanical bond and electrical connectivity between the TiABs, concrete substrate, and protected reinforcement.

The research program combines electrochemical and structural performance evaluations. Electrochemical testing, including material characterization, small-scale prism experiments, and large-scale beam specimens subjected to active corrosion, demonstrated that TiABs installed with ECSG function effectively as ICCP anodes, achieving stable operating currents, predictable polarization behavior, and compliance with accepted cathodic protection performance criteria. Structural tests included bond (pullout) experiments and large-scale flexural and shear beam tests of specimens representative of vintage RC bridge construction practices. Results confirmed that ECSG-bonded TiABs satisfy development length requirements, restore flexural and shear capacity, and maintain predictable failure modes consistent with established NSMR design practices.

Collectively, the results demonstrate that near-surface mounted TiABs can be deployed as a true dual-purpose system, simultaneously restoring structural capacity and enabling long-term corrosion protection. This report synthesizes the findings into a system-level assessment and provides a foundation for future development and implementation of integrated strengthening and preservation strategies for aging transportation infrastructure.

Keywords: reinforced concrete; corrosion; cathodic protection; near-surface mounted reinforcement; titanium alloy bars; infrastructure rehabilitation

INTRODUCTION

Background and Motivation

A significant portion of the U.S. reinforced concrete (RC) transportation infrastructure is approaching or exceeding its original design life. Many existing bridges and structural elements exhibit a combination of structural capacity deficiencies and active corrosion of embedded steel reinforcement, primarily driven by chloride exposure (ACI 222, 2019; Jones, 1996). While these deterioration mechanisms are closely linked, they are typically addressed through separate rehabilitation strategies.

Near-surface mounted reinforcement (NSMR) techniques are widely used to restore flexural and shear capacity in existing RC structures. The most common approach deploys fiber reinforced materials which have become standardized (ACI Committee 440, 2024; Parvin and Shah, 2016). Titanium alloy bars (TiABs) have emerged as an effective NSMR material, offering high strength, durability, and established design guidance for bridge applications (AASHTO, 2020; Higgins, et al., 2015; Higgins et al. 2017; Knudtsen and Higgins, 2017; Vavra and Higgins, 2017). However, NSMR systems alone do not mitigate corrosion of the existing reinforcement.

Impressed current cathodic protection (ICCP) is a proven method for mitigating corrosion in chloride-contaminated RC structures (NACE International, 2000; Byrne, Holmes and Norton, 2016). Conventional ICCP systems use titanium-based anodes that provide long-term electrochemical stability (Segan et al., 1982; NACE International, 2016; Funahashi, 2013) but serve no structural function. The lack of integration between strengthening and corrosion protection increases construction complexity and limits rehabilitation efficiency.

This research advances a novel integrated rehabilitation concept in which TiABs are used simultaneously as structural strengthening elements and ICCP anodes. This dual-function approach has the potential to restore structural capacity while also providing long-term corrosion protection in a single system. Limited prior work has considered such an approach and only with fiber reinforced materials (Bahekar and Gadve, 2017; Su et al., 2019).

Research Objectives

The overarching objective of this research was to develop and validate a dual-function NSMR system capable of providing both structural strengthening and impressed current cathodic protection for reinforced concrete transportation infrastructure.

Specific objectives included:

- Development of an electrically conductive structural grout (ECSG).
- Evaluation of electrochemical performance of TiABs as ICCP anodes.
- Quantification of bond behavior and development characteristics of ECSG-bonded TiABs.
- Demonstration of flexural and shear strengthening through large-scale beam tests.
- Assessment of system-level compatibility between structural and electrochemical functions.
- Synthesis of findings to support future development and eventual deployment.

SYSTEM DESCRIPTION

The integrated rehabilitation system developed in this research combines NSMR for structural strengthening with ICCP for corrosion mitigation using a single set of multifunctional components. The system is centered on the use of high-strength TiABs that serve simultaneously as structural reinforcement and electrochemical anodes, enabled with a specially developed ECSG. Together, these components form a unified strengthening and preservation system for reinforced concrete transportation infrastructure.

Titanium Alloy Bars as Dual-Function Elements

The primary reinforcing elements in the system are TiABs manufactured in accordance with ASTM B1009-24 (2024), typical of Ti-6Al-4V alloy (Grade 5). These bars possess high yield strength, corrosion resistance, and surface deformations that enhance mechanical bond when used in NSMR applications. Examples of the TiABs used in this research are shown in Fig. 1. The material properties of all the reinforcing bars, both titanium and steel, used in this study are reported in Table 1. It is noted that the TiAB size number corresponds similarly to that of conventional reinforcing steel and the class number corresponds to the minimum specified yield stress in ASTM B1009-24 (2024).

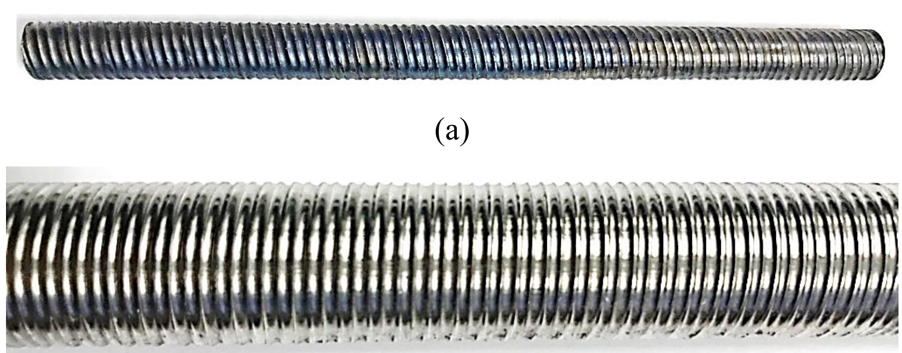

(a)

(b)

Figure 1. TiAB profiles (a) #2 bar; (b) #5 bar.

Table 1: Properties of the titanium and steel bars used in the study.

Property	Gr. 40 Steel (#4)	Gr. 60 Steel (#9)	TiAB B1009 (#2)	TiAB B1009 (#5)
Nominal diameter, in [mm]	0.50 [13]	1.125 [29]	0.25 [6]	0.625 [16]
Effective cross-sectional area, in^2 [mm^2]	0.20 [129]	1.00 [645]	0.049 [32]	0.31 [200]
Minimum yield stress, ksi [MPa]	40 [275]	60 [415]	130 [900]	130 [900]
Actual yield stress, ksi [MPa]	52 [359]	68 [476]	136.3 [984]	142.7 [984]
Actual tensile strength, ksi [MPa]	81 [558]	102 [703]	150 [1034]	154 [1062]
Nominal modulus of elasticity, ksi [GPa]	29,000 [200]	29,000 [200]	15,550 [107]	15,500 [107]
Elongation, %	28	15	20	19

In the system described herein, TiABs are installed as near-surface mounted reinforcement in grooves cut into the concrete cover as illustrated in Fig. 2a and 2b, providing supplemental longitudinal or transverse reinforcement depending on the targeted structural deficiency. Unlike conventional NSMR systems, in which the reinforcing bars are electrically isolated from the surrounding concrete, the TiABs in this system are intentionally configured to remain electrically active, allowing them to function as ICCP anodes while simultaneously carrying structural load.

a) b)

Figure 2. Grooves being cut into concrete surface with diamond blade circular saw; b) finished and cleaned grooves ready for bonding NSMR (shear application shown).

The use of TiABs as ICCP anodes represents a departure from traditional cathodic protection practice, which typically employs commercially pure titanium (Grades 1 or 2) coated with mixed metal oxides (MMO) in non-structural forms such as ribbons, meshes, or wires. In contrast, the TiABs used here are uncoated, high-strength structural elements. Their successful deployment as anodes therefore requires careful consideration of electrical connectivity, current distribution, and interface behavior, all of which are addressed through design and material selection.

Electrically Conductive Structural Grout

A critical enabling component of the system is the ECSG used to bond the TiABs into the NSMR grooves. Conventional NSMR installations typically rely on epoxy adhesives, which provide excellent mechanical bond but electrically isolate the reinforcing bars from the surrounding concrete and embedded steel reinforcement. Such isolation precludes the use of NSMR bars as ICCP anodes.

The ECSG was developed to satisfy dual performance requirements: 1) provide sufficient mechanical strength to enable bond and load transfer between the TiABs and the concrete substrate to meet structural design criteria, and 2) maintain low electrical resistivity to permit current flow between the TiABs and the embedded reinforcing steel for ICCP criteria (NACE International, 2000; Glass, 1999).

Two commercially available high-strength grouts were selected as options for installing TiABs in surface grooves of structural elements. Non-shrink grouts were required to satisfy both the structural (NSRM) and electrical connectivity (ICCP) requirements. The commercial grouts were repair grouts from commonly known and accessible manufacturers. The grouts were chosen for their sulfate resistance for marine environments, freeze/thaw resistance, fluid consistency over a 30-minute working time, high placement versatility, and their recommended use for the placement of anchors and dowels.

Variables considered in the grout design included the brand of commercial grout, carbon fiber content, carbon fiber length, carbon black content, methyl cellulose content, and quantity of high range water reducer (HRWR). Carbon fibers (CFs) were incorporated in the grout mixtures based on volume percentage to increase electrical conductivity of the grouts (Sun et al., 2011; Sassani et al., 2017). The use of carbon fibers in a cementitious mixture required the addition of a dispersion agent to prevent fibers from clumping together. The dispersion agent used was methyl cellulose, which was added to the mixtures based on percent by weight of grout. Carbon black was also considered as a material that could impact the conductivity (or resistivity) of the grout, and it was combined with carbon fibers in the grout mix by percent volume.

The commercial grouts exhibited compressive strengths suitable for structural applications and bulk electrical resistivity values significantly lower than those of conventional concrete, enabling efficient current transfer for ICCP operation. Compressive strength testing was conducted in accordance with ASTM C109/C109M-16a (ASTM International, 2016), and bulk electrical resistivity was measured in accordance with ASTM C1876-19 (ASTM International, 2019). Average 28-day compressive strength and resistivity values are presented in Table 2.

Table 2: Average compressive strength and average bulk resistivity of commercial grouts considered in research program.

Commercial Grout	Avg. 28 Day Compressive Strength (psi) [MPa]	Avg. 28 Day Bulk Resistivity (kΩ-cm)
#1	9,532 [65.7]	15.36
#2	10,008 [69]	4.65

Carbon fiber was added to further increase the conductivity of the grout. Three different lengths of carbon fibers were used to determine the effect on both resistivity and compressive strength. All of the carbon fibers were unsized, milled polyacrylanitrile fiber with a carbon content of 94% or greater in accordance with ASTM D5291-16 (ASTM 2016). Carbon fibers have a diameter of 7-9 microns and a tensile strength of 2.0 to 3.8 GPa [290 to 551 ksi]. The NSMR design application for the grout prescribed the use of a 1 in. [25.4 mm] by 1 in. [25.4 mm] square groove and a ½ in. [13mm] by ½ in. [13mm] square groove for the placement of #5 and #2 TiABs, respectively. Due to the small groove sizes, short CF lengths were considered. The fiber lengths ranged from 350 microns to 6 mm. The recommended amount of carbon fiber content in concrete is less than 1% by total volume of grout (Sassani et al., 2017). This carbon fiber content recommended in the research considers percentage volume for concrete, which includes large aggregates in its composition, so the volume percentage was adjusted for grout, by correcting for the absence of large aggregates. Volume percentages considered were 0.1%, 0.2%, and 0.4% for the carbon content in the grout mix. Table 3 provides the details of the grout matrix based on carbon fiber size and content. The salient performance characteristics of the CF modified grouts are shown in Table 4. The strength results in Table 4 are from six (6) replicate cube specimens for each mix combination, while the electrochemical properties are from grout cylinders as shown in Figure 3.

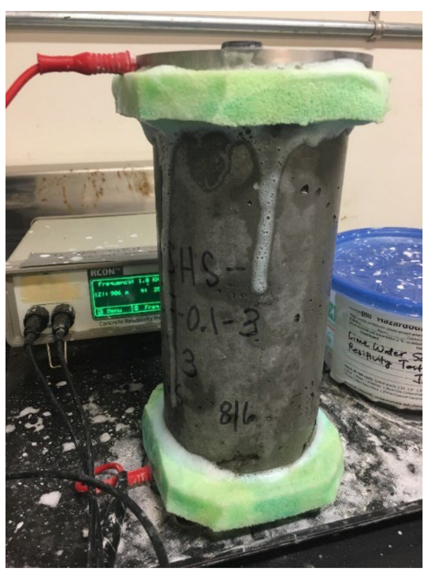

Figure 3. Grout cylinder undergoing bulk resistivity test.

The final mix consisted of Commercial Grout #2, methyl cellulose dispersion agent, 0.4% CF content with 0.24 in. [6 mm] long fibers, HRWR agent, and is herein referred to as the ECSG which was used for all subsequent experiments.

Table 3: Carbon fiber content matrix.

Grout	Control (No Fibers)	Carbon Fibers (CF)			
		% CF by volume	6 mm	3 mm	Milled (350 micrometers (µm))
Commercial Grout #1	1-C	0.1	1-CF-0.1-6	1-CF-0.1-3	1-CF-0.1-M
		0.2	1-CF-0.2-6	1-CF-0.2-3	1-CF-0.2-M
		0.4	1-CF-0.4-6	1-CF-0.4-3	1-CF-0.4-M
Commercial Grout #2	2-C	0.1	2-CF-0.1-6	2-CF-0.1-3	2-CF-0.1-M
		0.2	2-CF-0.2-6	2-CF-0.2-3	2-CF-0.2-M
		0.4	2-CF-0.4-6	2-CF-0.4-3	2-CF-0.4-M

Table 4: Characteristics of different CF additions to Commercial Grout #2.

Carbon Fiber Content (% Volume)	**Carbon Fiber Size (mm)**	**Average 28 Day Compressive Strength (psi) [MPa]**	**Average 28 Day Bulk Resistivity (kΩ-cm)**	**% Change in Average 28 Day Compressive Strength**	**% Change in Average 28 Day Bulk Resistivity**
0.1	~0.350 (milled)	8356 [57.6]	5.27	-17%	13%
	3	6296 [43.4]	3.48	-37%	-25%
	6	6987 [48.2]	4.22	-30%	-9%
0.2	~0.350 (milled)	8425 [58.1]	2.37	-16%	-49%
	3	8561 [59]	0.40	-14%	-91%
	6	9214 [63.5]	2.28	-8%	-51%
0.4	~0.350 (milled)	8963 [61.8]	1.86	-10%	-60%
	3	9279 [64]	0.29	-7%	-94%
	6	8744 [60.3]	0.16	-13%	-96%

Electrical Connectivity and ICCP Integration

Electrical integration of the system requires controlled connectivity between the TiAB anodes and the embedded steel reinforcement while allowing selective isolation of reinforcement components for testing and evaluation. Electrical connections to both the TiABs and steel rebar were established externally using mechanically secured and corrosion-protected wiring as illustrated in Fig. 4a to c. The exposed ends of the longitudinal reinforcing steel bars were drilled and tapped to facilitate external connection to copper wiring. Although the stirrups did not have external access during casting, access holes were drilled through the concrete cover after curing to expose the side of selected stirrups. These stirrups were drilled and tapped to establish external electrical connections while minimizing the risk of corrosion at the connection interface. The longitudinal TiABs were drilled and tapped at the external side of the hook bend, allowing electrical connections to protrude slightly from the beam surface. These connections allow the TiABs to be energized as anodes within an ICCP system and the reinforcing steel to act as the cathode.

a) b) c)

Figure 4. Examples of electrical connections for ICCP application a) #2 TiAB, b) Steel stirrup, and c) steel longitudinal steel.

Near-Surface Mounted Installation Configuration

Installation of the integrated system follows established NSMR construction practices with minor modifications to accommodate the ECSG and electrical requirements. Grooves are cut into the concrete cover at prescribed locations and dimensions based on bar size and reinforcement function. The TiABs are placed within the grooves and bonded using ECSG rather than epoxy, with care taken to ensure full encapsulation and consolidation of the grout. Electrical leads are attached to the TiABs prior to grout placement. The resulting configuration provides a low-profile retrofit that preserves structural clearances while enabling long-term corrosion protection.

System-Level Integration

At the system level, the integrated NSMR–ICCP approach provides a single intervention that addresses both immediate structural deficiencies and long-term durability concerns. The TiABs restore flexural and/or shear capacity, the ECSG ensures adequate bond and electrical continuity, and the ICCP system mitigates ongoing corrosion of the embedded reinforcement. The system is inherently modular and adaptable, allowing reinforcement layout, current density, and electrical connectivity to be tailored to specific structural configurations and deterioration conditions.

This integrated configuration forms the basis for the experimental investigations presented in subsequent sections, including electrochemical performance evaluation, bond and structural testing, and an integrated assessment of combined strengthening and cathodic protection behavior.

EXPERIMENTAL METHODS

Small-Scale Prisms

Small-scale prism specimens were used to evaluate the electrochemical performance of the integrated system and establish the operating parameters for the subsequent beam specimens. Two reinforced concrete prisms were cast using an ordinary portland cement (OPC) concrete mixture with a water-to-cement ratio (w/c) of 0.55. To promote active corrosion of the embedded steel reinforcement, the mixing water contained 1.5% chlorides in the form of sodium chloride (NaCl). The concrete mixture was selected to closely represent materials commonly used in reinforced concrete bridge construction during the mid-twentieth century. Type I/II Portland cement was used. The concrete mixture proportions are summarized in Table 5.

Table 5: Small-scale prism concrete proportions.

water/cement ratio	0.55
Required concrete volume (ft^3)	1.85
Water (lbs/yd^3)	419
Cement (lbs/yd^3)	618
Coarse aggregate (lbs/yd^3)	1239
Fine aggregate (lbs/yd^3)	1533
NaCl (lbs/yd^3)	15.3

Each prism had nominal dimensions of 8 in. × 6 in. × 18 in. (200 mm × 150 mm × 460 mm). The reinforcement layout consisted of two No. 9 Grade 60 carbon steel reinforcing bars and two No. 4 Grade 40 carbon steel reinforcing bars. All reinforcing bars were 18 in. (460 mm) long and were cast longitudinally within the prism, extending approximately 1 in. (25.4 mm) beyond one end of the concrete specimen to allow for external electrical connections. Prior to casting, the exposed ends of the reinforcing bars were drilled and tapped to facilitate electrical connection for impressed current cathodic protection (ICCP). After casting, fasteners were installed in the tapped bar ends, and copper wire was tightly wrapped around the fasteners to externally connect the reinforcing bars within the prism. The exposed ends of the reinforcing bars were then coated with epoxy to prevent localized corrosion and unintended current loss. A schematic of the prism cross section and reinforcement layout is shown in Figure 5.

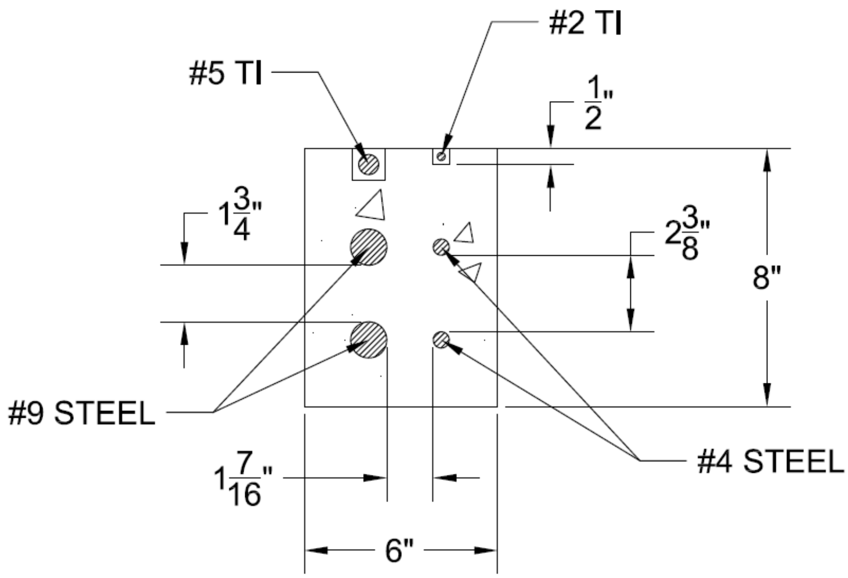

Figure 5. Schematic of small-scale prism specimen cross section (1 in. = 25.4 mm).

The prism specimens were cured under wet burlap for 28 days. After curing, grooves were cut into the concrete surface for placement of TiABs. The #5 TiABs were installed in grooves measuring 1 in. × 1 in. (25.4 mm × 25.4 mm), and the #2 TiABs were installed in grooves measuring ½ in. × ½ in. (13 mm × 13 mm). The TiABs were bonded into the grooves using the ECSG. A completed prism specimen is shown in Fig. 6. After curing of the ECSG, ICCP tests were conducted with the specimens.

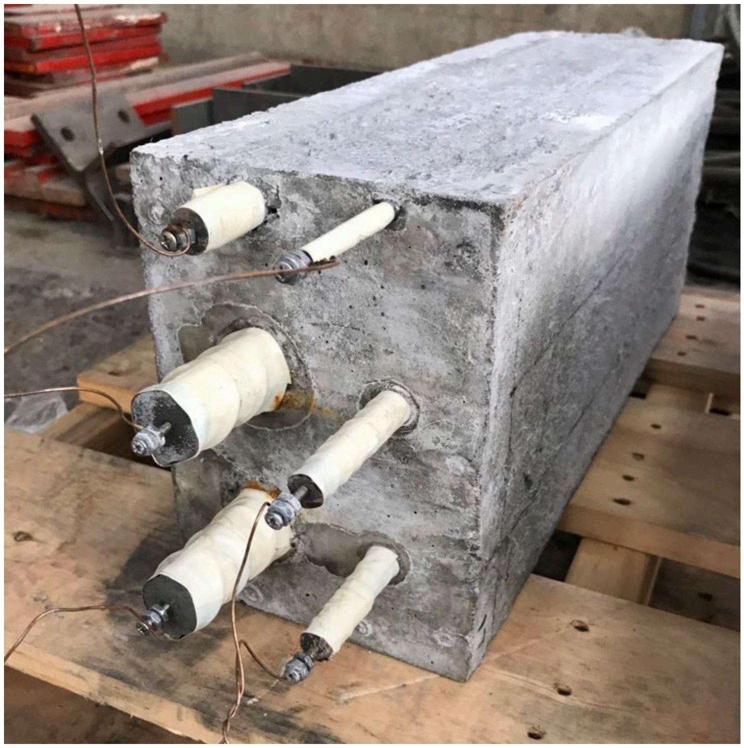

Figure 6. Photograph of completed small-scale prism specimen.

Large-Scale Beams

Two reinforced concrete beam specimens were designed, as shown in Figures 7 and 8. One specimen was proportioned to produce a flexural failure and was strengthened using #5 longitudinal TiABs (Flexural Specimen). The second specimen was proportioned to produce a diagonal-tension (shear-dominated) failure in half of the beam and was strengthened using #2 transverse TiABs (Shear Specimen). The specimens differed in span length and reinforcement configuration to achieve the intended failure modes.

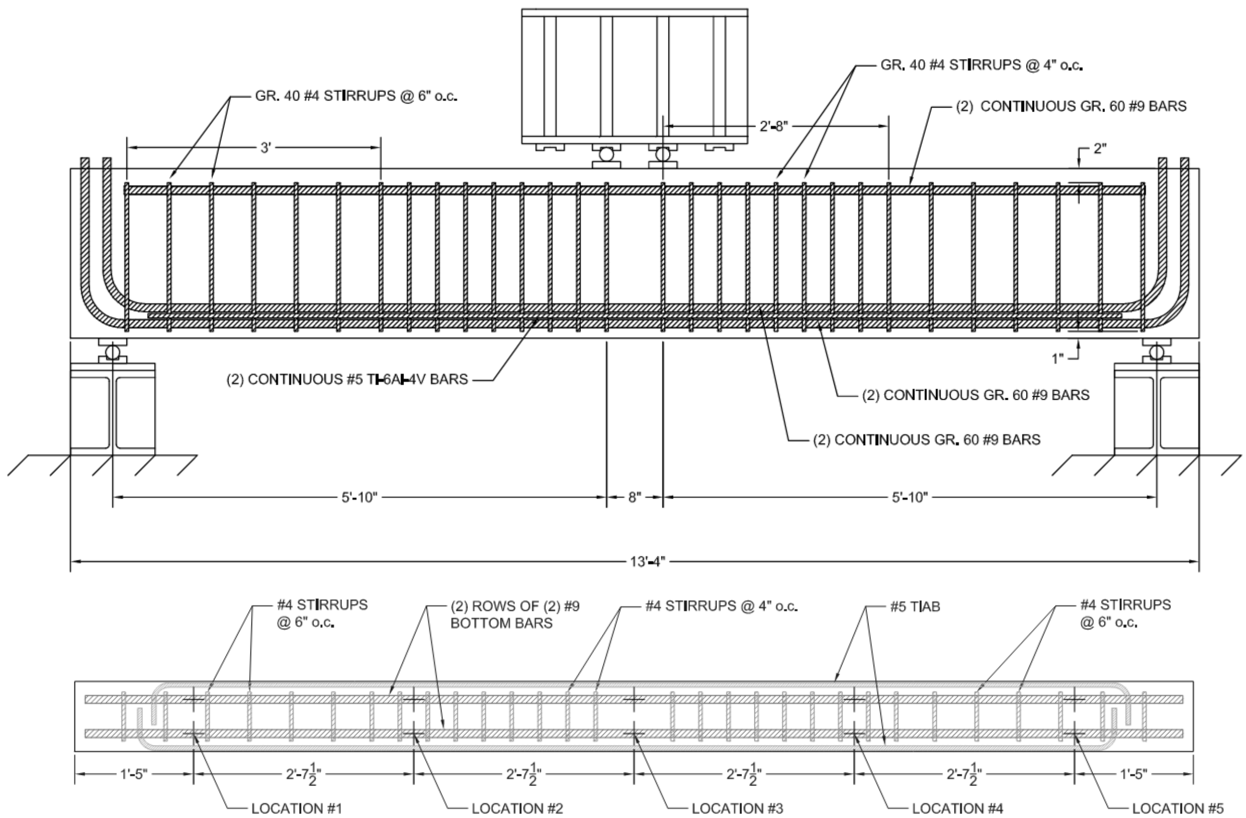

(a)

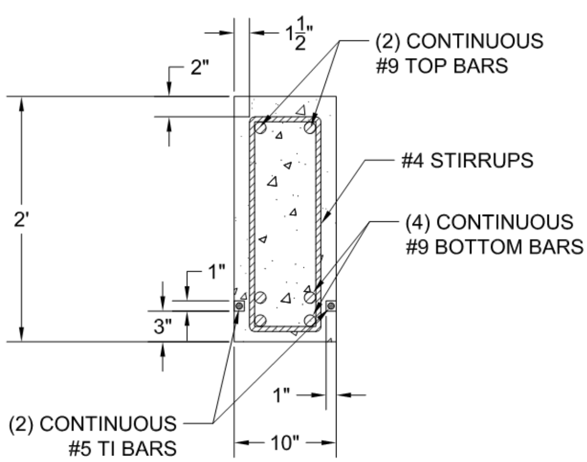

(b)

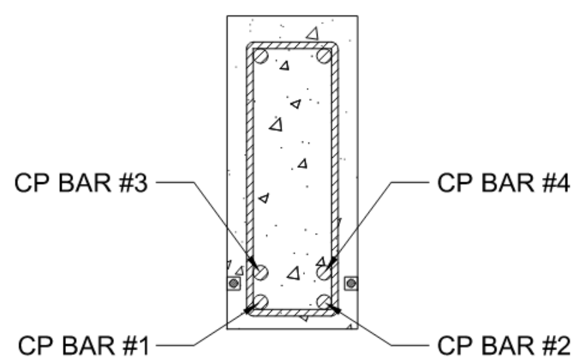

(c)

Figure 7. Flexural beam (a) span, (b) cross section, and (c) ICCP bar numbers.

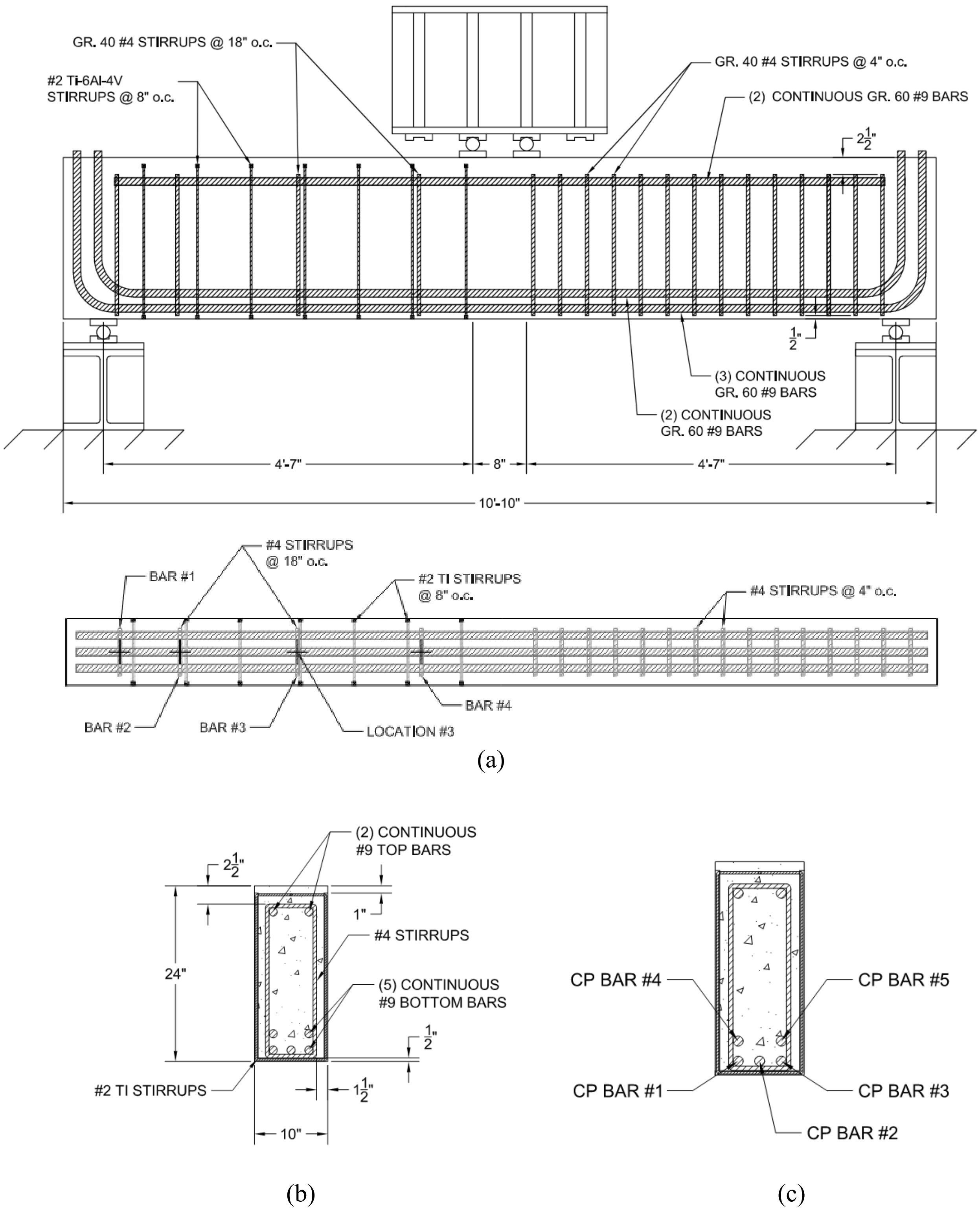

Figure 8. Shear beam (a) span, (b) cross section, and (c) ICCP bar numbers.

Concrete for the NSMR-TiAB/ICCP beam specimens was supplied by a local ready-mix producer. The mixture was proportioned to replicate concrete commonly used in mid-twentieth-century bridge construction and was consistent with the prism study described above. The specified minimum compressive strength was 3300 psi [22.8 MPa]. To induce active corrosion of the embedded reinforcement, 1.5% chlorides (as NaCl) by mass of cement were added to the mixing water. The salt was introduced directly into the batch water in the ready-mix truck to ensure uniform distribution. Concrete mixture proportions are provided in Table 6.

Table 6: Beam specimen concrete mix proportions.

Material	Design Qty. per yd^3	Required	Batched	% Variation	% Moisture	Actual Water (gal)
¾ in. Agg.	1741 lb.	5342 lb.	5290 lb.	-0.97%	2.27% M	14
Sand	1392 lb.	4428 lb.	4420 lb.	-0.19%	6.04% A	30
OPC	470 lb.	1410 lb.	1397 lb.	-0.92%		
Daravair	1.40 oz.	4.20 oz.	4.00 oz.	-4.76%		
WRDA_64	23.50 oz.	70.50 oz.	68.00 oz.	-3.55%		
Cold Water	31 gal.	43 gal.	47 gal.	10.43%		47
NaCl	11.62 lb.	34.9 lb.	35.3 lb.	+1.25%		

Carbon steel reinforcement was used to replicate detailing typical of aging highway bridges. Because historical Intermediate Grade reinforcing steel corresponds approximately to modern Grade 40 steel, this grade was used where available. Grade 40, #4 rebar were used for stirrups. Larger diameter Grade 40 bars are no longer commercially available; therefore, #9 Grade 60 bars were used for longitudinal reinforcement, with bar sizing selected to approximate the intended strength levels. The longitudinal reinforcement was detailed with 90-degree hooks at the ends to prevent anchorage failure. The hook extensions were intentionally extended above the top surface of the beams to allow external electrical connection for ICCP.

Electrical connections were required to both the reinforcing steel and the TiABs for ICCP operation. Because the concrete was intentionally chlorinated to create a corrosive environment, external access to reinforcement was used to prevent deterioration of ICCP wiring within the beam as described previously. A potentiostat was connected to each longitudinal reinforcing bar at the hook extension protruding above the concrete surface.

To isolate the electrochemical response of specific reinforcement groups, individual reinforcing components were electrically insulated from one another. Although reinforcing bars in typical construction are in direct contact and tied with steel wire, this study required controlled isolation. Nylon tubing segments were placed around longitudinal bars at their intersections with transverse reinforcement to prevent electrical continuity. Plastic zip-ties were used instead of steel tie wire to assemble the cages as shown in Fig. 9. This configuration allowed individual bars or bar groups to be selectively incorporated into or excluded from ICCP application, enabling direct observation of the electrochemical response of flexural tension steel and stirrups independently. In selected configurations, top #9 longitudinal bars were intentionally connected to #4 stirrups using tie wire to permit controlled inclusion of compression reinforcement and stirrups in ICCP testing.

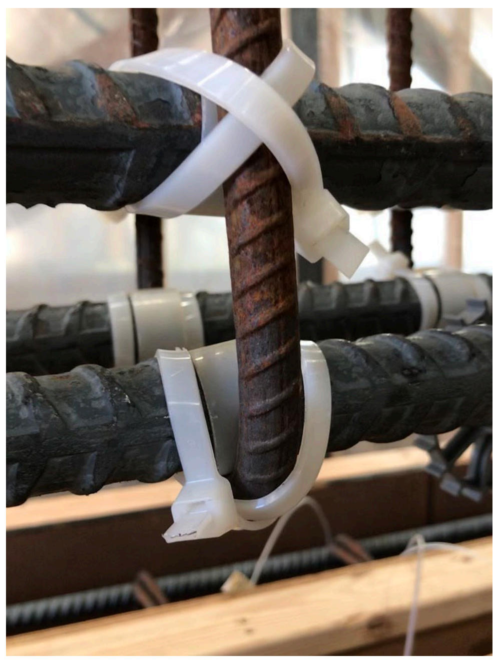

Figure 9. Example of nylon tubing and plastic zip ties used to construct cage. These allowed electrical isolation or inclusion of the different rebars in the ICCP system.

The beams were cured under wet burlap for 14 days prior to formwork removal and cutting of NSMR grooves. The measured 28-day compressive strength was 3387 psi [23.4 MPa], and the compressive strength at the time of testing was 3839 psi [26.5 MPa] [16]. Bulk resistivity of the concrete, measured from cylinders cast alongside the beams, was 4.96 kΩ·cm. The ECSG exhibited a 28-day compressive strength of 8600 psi [59.3 MPa] [13] and a bulk resistivity of 0.875

kΩ·cm. Figure 10 shows the beam specimens following installation of the near-surface mounted TiABs. The beams were subsequently subjected to electrochemical and structural testing.

(a)

(b)

Figure 10. (a) Flexural beam specimen with TiABs (shown inverted for ease of TiAB installation); (b) Shear beam specimen with TiABs (also shown inverted for ease of TiAB installation).

ELECTROCHEMICAL PERFORMANCE

Integrated NSMR-ICCP System

The electrochemical performance of the integrated NSMR and ICCP system was evaluated to verify that TiABs, when installed using ECSG, can function effectively as ICCP anodes. The electrochemical assessment focused on material resistivity, polarization behavior, current demand, and compliance with accepted cathodic protection performance criteria. Electrochemical performance was first evaluated for small-scale prism specimens and then extended to the large-scale beam specimens.

Small-Scale Prisms

The prism specimens were used to determine the appropriate voltage and current ranges required to achieve cathodic protection of the embedded steel reinforcement. Bulk electrical resistivity measurements showed that the prism concrete exhibited an average resistivity of 3.77 kΩ·cm, while the ECSG exhibited an average resistivity of 0.42 kΩ·cm. Open-circuit half-cell potentials (HCPs) of the prism specimens were measured to assess the corrosion state of the embedded reinforcing steel. HCP measurements were performed using a high-impedance voltmeter and a saturated calomel electrode (SCE) in accordance with ASTM C876. The inclusion of premixed chlorides in the concrete was intended to induce active corrosion of the embedded reinforcement. The measured HCP of the embedded rebars were stable between -325 to -400 mV (SCE), which is indicative of active corrosion, as expected.

In conventional ICCP systems for reinforced concrete structures, recommended current densities to achieve cathodic protection typically range from 0.6×10^{-7} A/cm² to 2.5×10^{-7} A/cm². Because ICCP performance is system-specific, a more rigorous approach for selecting the applied current density was adopted in this study through characterization of the polarization behavior of the embedded reinforcing steel. Anodic polarization scans were performed, and the linear region of the cathodic portion of the polarization curve was used to identify an appropriate operating potential range and corresponding current density, consistent with established ICCP guidelines.

Polarization scans were conducted using a stainless-steel plate counter electrode placed on the concrete surface directly above the reinforcing bar being evaluated, as illustrated in Figure 11. To improve electrical contact between the counter electrode and the concrete surface, a sponge saturated with a conductive solution was positioned between the electrode and the concrete. All polarization testing was performed using a Gamry Interface 3000 potentiostat, with the embedded reinforcing steel serving as the working electrode, a saturated calomel electrode (SCE) as the reference electrode, and the stainless-steel plate as the counter electrode. Representative polarization scans are shown in Figure 12.

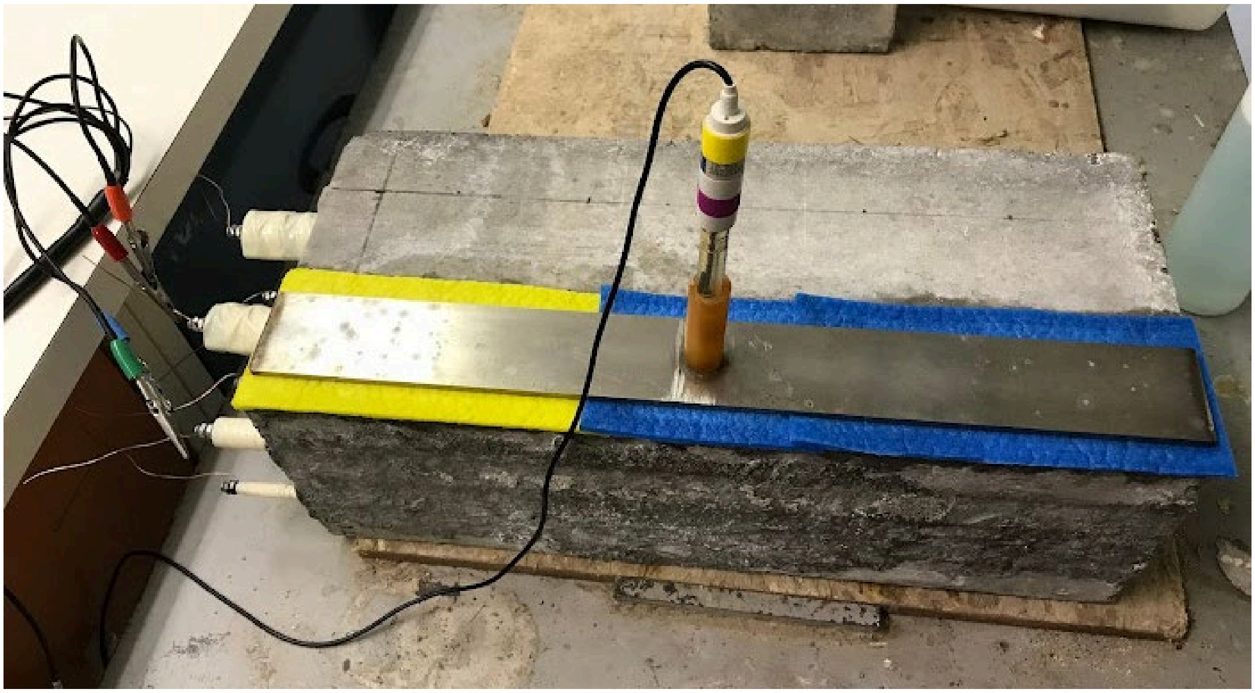

Figure 11. Polarization scans being taken on small-scale prism specimen.

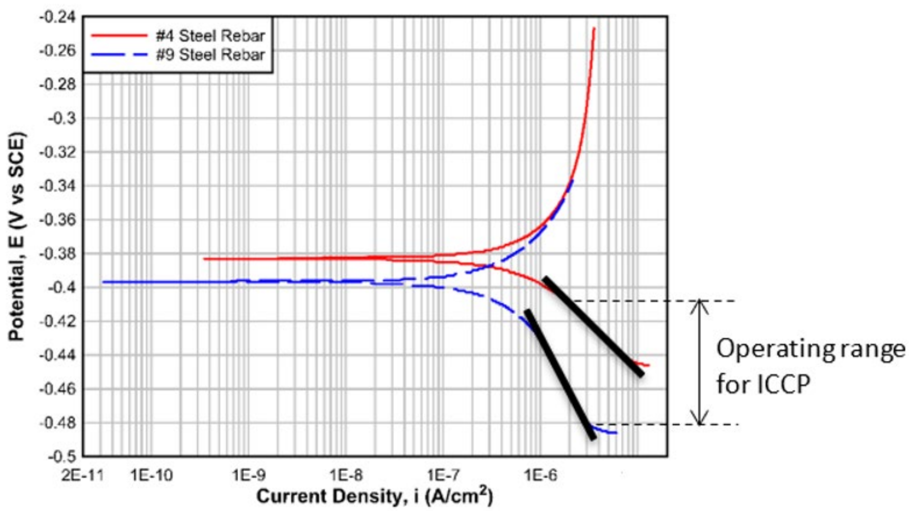

Figure 12. Potentiodynamic scan of steel reinforcing bars in concrete prism specimen.

The linear segment of the cathodic portion of the polarization curves defines the cathodic potential range appropriate for ICCP operation. Although the # 4 and # 9 reinforcing bars exhibited slightly different polarization behavior, the linear region corresponded to a potential range of approximately –410 mV to –480 mV. Potentials more negative than –480 mV resulted in loss of linearity in the polarization response. The corresponding current densities within the linear cathodic range were approximately 1×10^{-6} A/cm² to 7×10^{-6} A/cm².

In practice, the current densities required during ICCP operation of the NSMR system using TiAB anodes were higher than those predicted by the potentiodynamic scans conducted with the stainless-steel counter electrode and conductive sponge (Figure 11). This discrepancy is attributed to additional resistance introduced by the ECSG and the grout-concrete interface, which were not present in the polarization scan configuration. Furthermore, because the TiABs were not MMO coated, higher operating currents may have been required to achieve equivalent cathodic polarization. Nevertheless, the polarization scans, like that of Figure 12 provided an initial basis for selecting the ICCP operating current. A series of trial ICCP runs was subsequently conducted to refine and finalize the applied current level. After several trials, the operating current for the ICCP application was selected as 4.40 mA, which corresponds to a 1.67×10^{-5} A/cm^2 current density on the protected rebar surface. This is higher than typical ICCP current densities used in conventional cathodic protection of reinforced concrete structural elements.

After selection of the operating current, ICCP was initiated following one hour of half-cell potential (HCP) monitoring to confirm stable open-circuit corrosion conditions and to ensure that prior ICCP iterations had not influenced the measurements. Following this baseline period, ICCP was applied and maintained for five (5) hours using a Gamry Interface 3000 potentiostat.

During ICCP operation, HCP measurements were recorded to monitor polarization of the embedded reinforcing steel. Measured potentials ranged from –450 mV (SCE) to –550 mV (SCE), depending on location. Although some measured potentials were more negative than the target range identified from the linear segment of the cathodic polarization curve, they remained stable and above hydrogen evolution potentials. The stability of these potentials also suggests that the electrical resistivity and chemical characteristics of the grout surrounding the TiABs did not change significantly during ICCP operation. It is noted, however, that these laboratory tests were short in duration relative to field applications, and long-term performance requires further investigation.

After five (5) hours of continuous ICCP operation, the applied current was terminated, and depolarization monitoring began. HCP measurements were taken at the concrete surface above each reinforcing bar at ten (10)-minute intervals over a four (4)-hour period to evaluate compliance with the 100 mV depolarization criterion. Typical measured potential decay for the #9 reinforcing bars following ICCP interruption is shown in Figure 13. As indicated in the figure, all locations exhibited depolarization of at least 100 mV within four (4) hours, satisfying the ICCP acceptance criterion. The results also suggest that the applied current could have been reduced while still meeting the 100 mV depolarization requirement. In some locations, cathodic potentials exceeded –485 mV (SCE), indicating that operation within a lower portion of the polarization-derived range may have been sufficient to achieve effective protection.

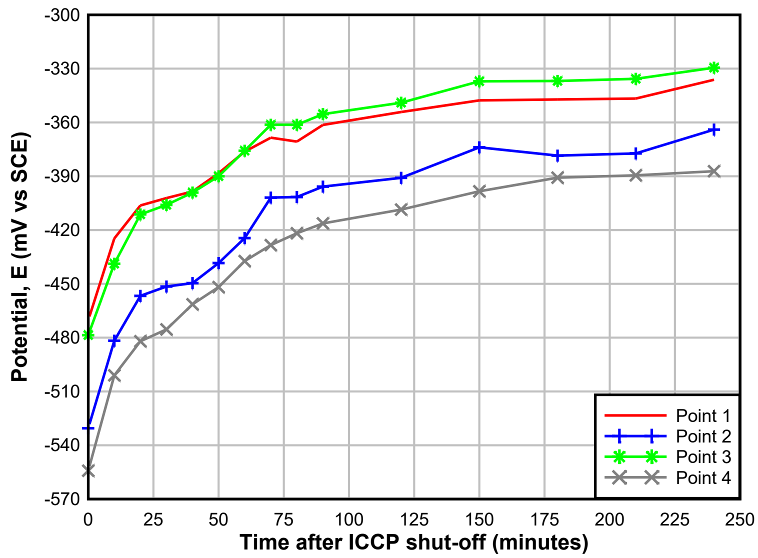

Figure 13. Depolarization of #9 steel reinforcing bars in test prism after ICCP current is terminated.

Beam Specimens

Flexural Beam Methods and Results

Prior to ICCP application, electrical isolation of the bottom longitudinal reinforcing bars was verified. In the flexural beam, the four #9 longitudinal reinforcing bars were externally connected using copper wire and attached to the potentiostat as the working electrode. The two #5 longitudinal TiABs were externally connected and served as the counter electrode (anode).

Half-cell potential (HCP) measurements were conducted on the flexural beam specimen prior to ICCP implementation to establish the corrosion state of the embedded reinforcement. All HCP measurements indicated active corrosion of the reinforcing steel under open-circuit conditions.

Following baseline HCP assessment, polarization scans were performed, as illustrated in Figure 14. A representative polarization curve for a longitudinal reinforcing bar in the flexural beam is shown in Figure 15. The linear segment of the cathodic portion of the polarization curve defined the potential range appropriate for ICCP operation.

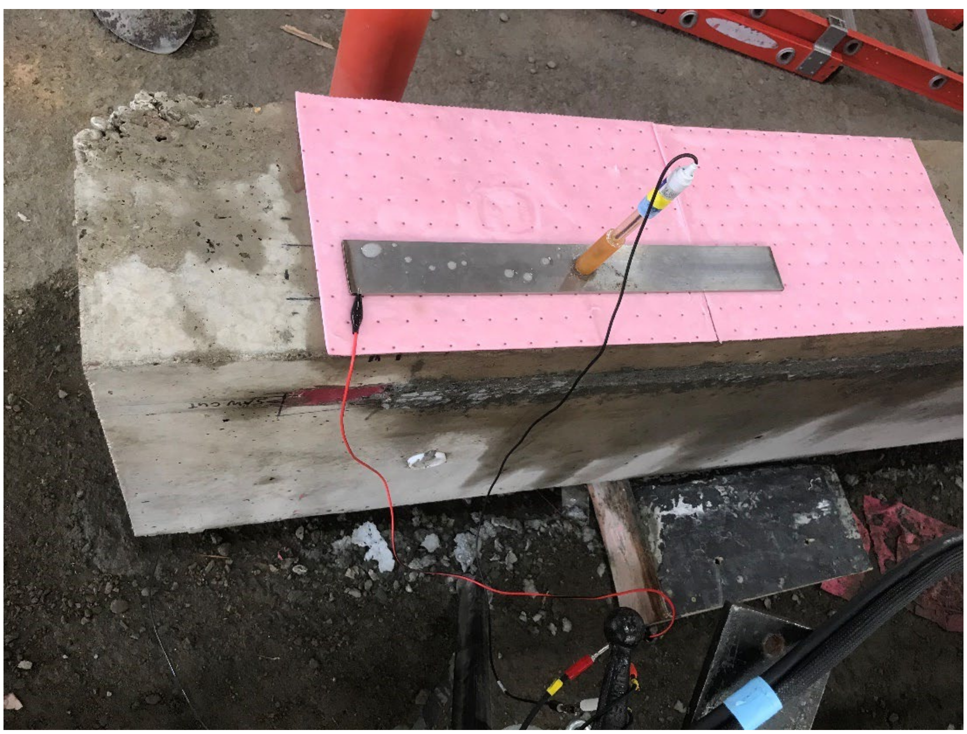

Figure 14. Polarization scan of flexural beam specimen.

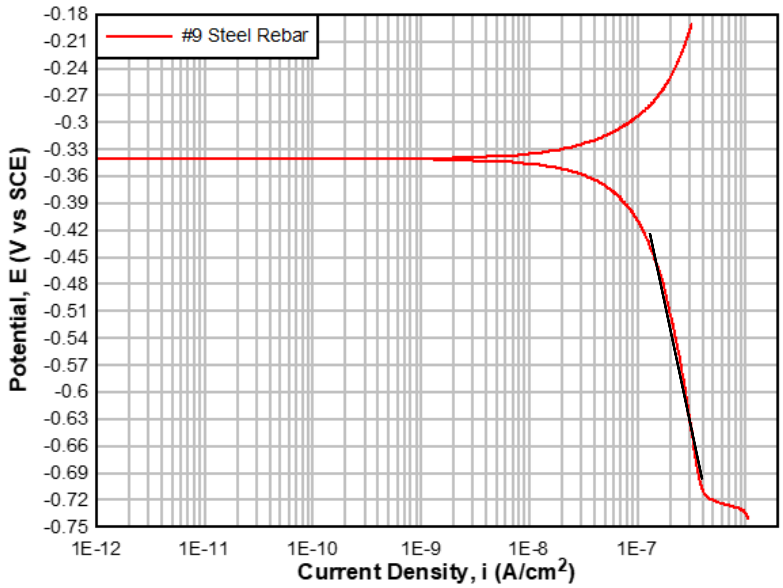

Figure 15. Example polarization scan of a #9 longitudinal steel reinforcing bar in the flexural beam at a measurement point. Other rebars and measurement locations showed similar patterns.

Although slight variations were observed among individual reinforcing bars and measurement locations, the linear cathodic region corresponded to potentials between approximately –425 mV and –700 mV (SCE). Potentials more negative than approximately –725 mV resulted in loss of linearity in the polarization response. The corresponding current density range associated with the linear region was approximately 1×10^{-7} A/cm² to 4×10^{-7} A/cm².

As in the prism tests, the polarization scans were conducted using a stainless-steel counter electrode placed on the concrete surface. Because this test configuration does not account for the distributed current path present in the NSMR system using TiAB anodes embedded in ECSG, it was anticipated that the current required during ICCP application would exceed that predicted directly from the potentiodynamic scans. Nevertheless, the polarization curves provided a rational lower bound for selecting the initial ICCP operating current.

ICCP was applied using a Gamry Interface 3000 potentiostat. An applied current of 143.9 mA was used, corresponding to a current density of 8.28×10^{-6} A/cm² on the protected steel surface. ICCP was sustained for five (5) continuous hours. During ICCP operation, HCP measurements were monitored to confirm polarization behavior and stability of the system.

Following five hours of ICCP operation, the applied current was interrupted. Depolarization was monitored through HCP measurements recorded at five evenly spaced locations along each of the four bottom longitudinal reinforcing bars (Figure 16 with the numbering was shown previously in Figure 4). Measurements were taken at 10-minute intervals over a four-hour period.

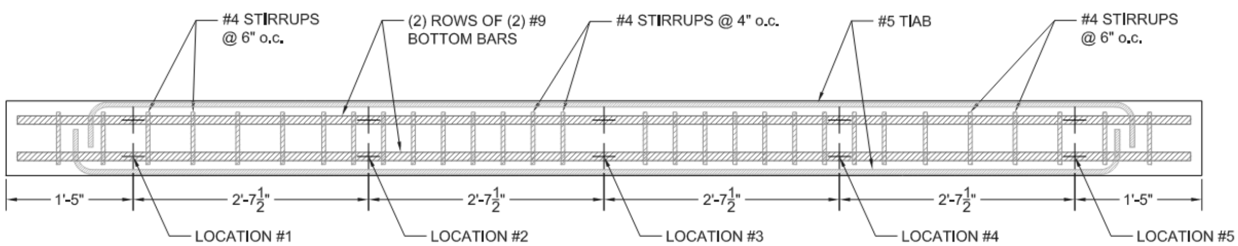

(a)

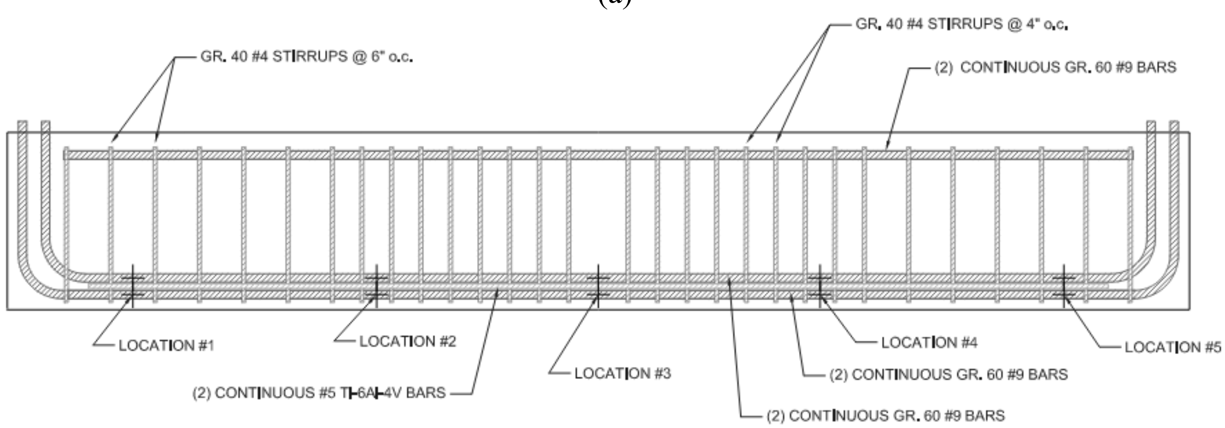

(b)

Figure 16. HCP measurement locations in the flexural beam a) Top view; b) Side view.

The applied current density required to achieve cathodic protection exceeded the lower bound predicted by polarization scans. This increase is attributed to additional electrical resistance introduced by the ECSG and grout-concrete interface, consistent with observations from the prism specimens. The applied current remained stable throughout ICCP operation and did not require significant adjustment (Figure 17), demonstrating that the uncoated TiABs were capable of sustaining the required current and that the ECSG functioned effectively as a conductive medium.

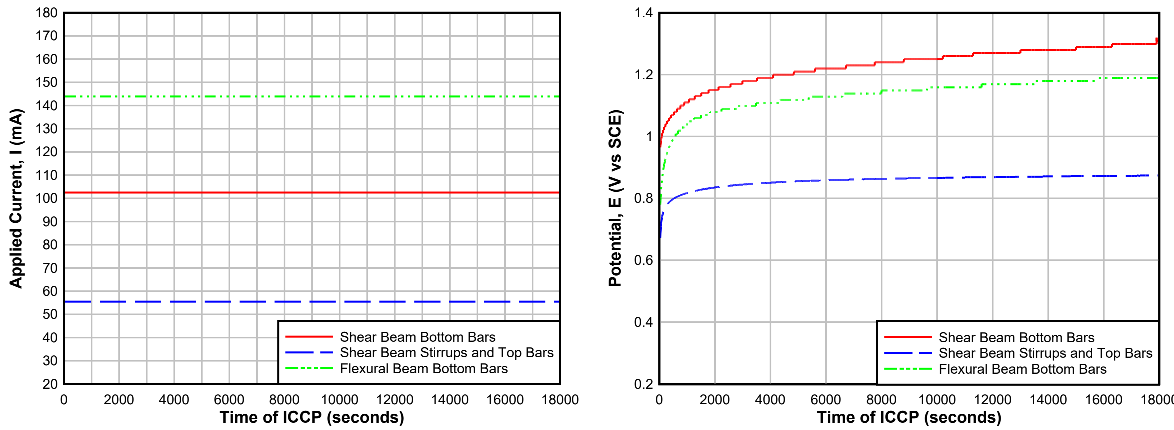

a) b)

Figure 17. a) Applied current; b) resulting potential in the flexural and shear beams during ICCP.

Measured potentials during ICCP ranged below portions of the target linear polarization region at some locations but remained stable and above hydrogen evolution potentials. The stability of measured potentials suggests that the electrical resistivity and chemical properties of the ECSG did not change substantially during the short-term laboratory test period. Following current interruption, all four longitudinal reinforcing bars exhibited depolarization of at least 100 mV within four hours (Figure 18), thereby satisfying the ICCP acceptance criterion. Due to the close proximity of the longitudinal TiABs to the reinforcing steel along the beam length, polarization response was relatively uniform across measurement locations.

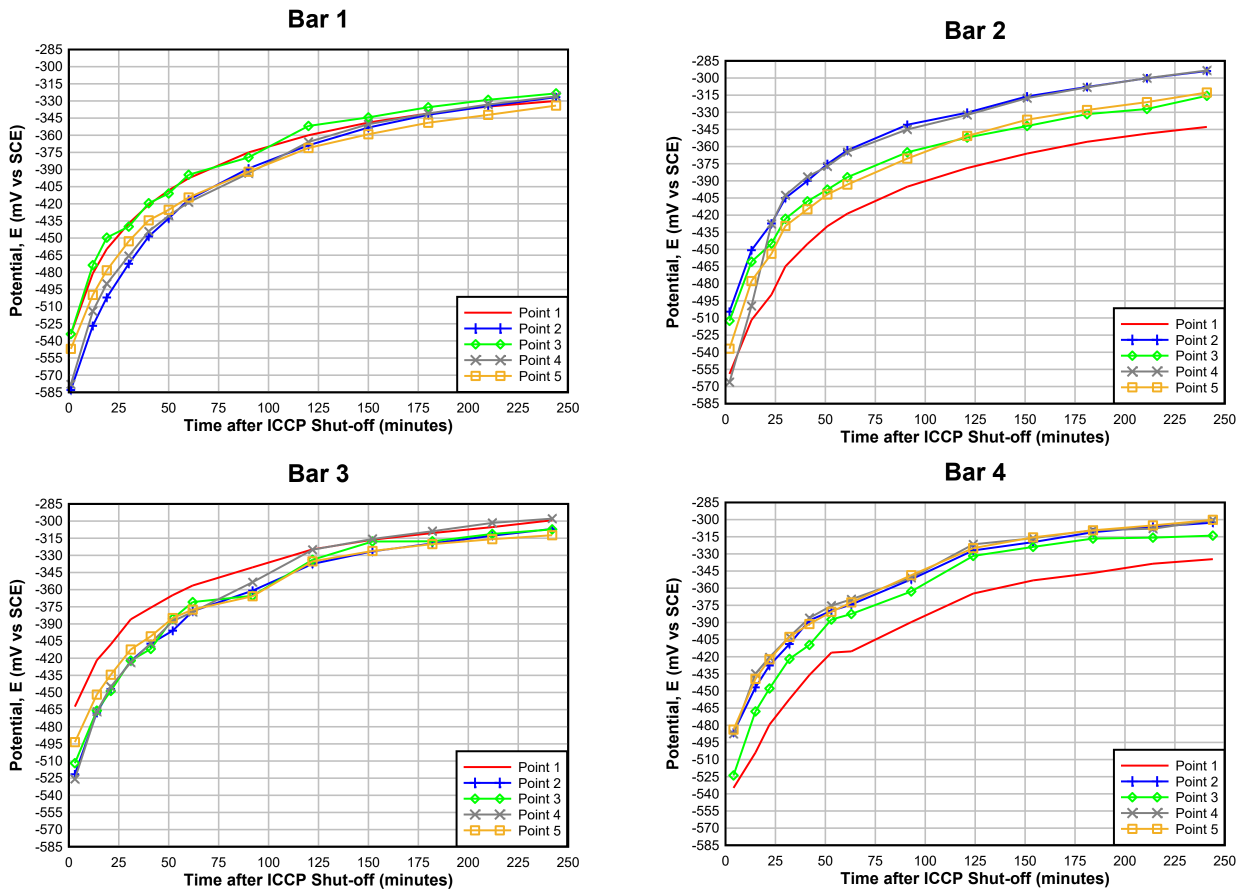

Figure 18. Depolarization of the different longitudinal reinforcing steel bars within the flexural beam after ICCP current is terminated.

The results show that the applied current exceeded the lower bound predicted by polarization scans, consistent with additional resistance introduced by the ECSG and grout-concrete interface. The applied current remained stable throughout ICCP operation as seen previously in Figure 16, demonstrating that uncoated TiABs were capable of sustaining the required current. Measured potentials during ICCP ranged below the targeted linear polarization region at some locations but remained stable and above hydrogen evolution potentials. This stability indicates that the grout resistivity and chemical characteristics did not change significantly during the test period. Following current interruption, all four longitudinal bars exhibited depolarization of at least 100 mV within four hours as seen in Figure 18, which satisfies the ICCP acceptance criterion. The relatively uniform TiAB placement along the beam length resulted in reasonably consistent polarization response across measurement locations.

Shear Beam Methods and Results

Baseline HCP measurements confirmed active corrosion in the reinforcing steel of the shear beam prior to ICCP application. Polarization scans were conducted to identify the cathodic operating range, which was consistent with that observed in the flexural beam (–425 mV to –700 mV, SCE), with corresponding current densities on the order of 10^{-7} A/cm². Because the specimen was purposely constructed in a way that could electrically isolate the bottom longitudinal bars from the steel stirrups with nylon tubing and plastic zip-ties, as described previously, two different ICCP configurations were evaluated:

1. Longitudinal bar protection: The #2 TiAB stirrups served as the counter electrode, and the five bottom # 9 longitudinal bars served as the working electrode. ICCP was applied at 102.5 mA, corresponding to 5.62×10^{-6} A/cm².
2. Stirrup and compression steel protection: The #2 TiAB stirrups served as the counter electrode, and the connected steel stirrups and two #9 top bars acted as the working electrode. ICCP was applied at 55.5 mA, corresponding to 1.11×10^{-5} A/cm².

In both cases, ICCP was applied for five (5) hours. Depolarization measurements were collected at 10-minute intervals over a four-hour period following current interruption. Longitudinal bar locations were distributed across front and back faces of the beam and TiAB stirrups were installed over only half the beam length, enabling evaluation of spatial effects. Measurement locations are shown in Figure 19 (bar numbers were identified in Fig. 7).

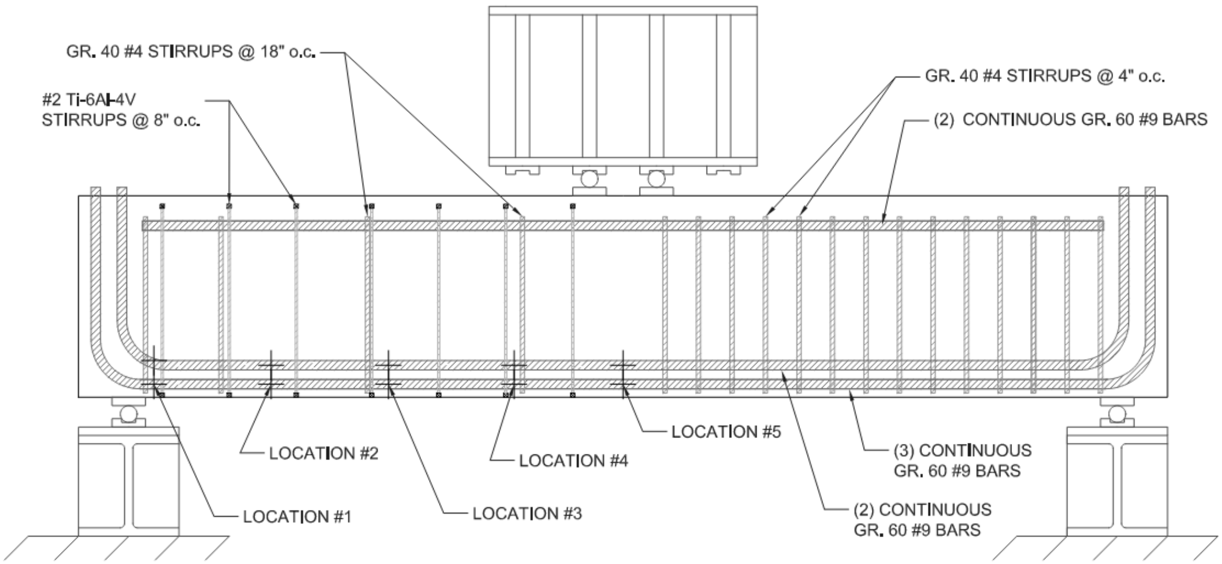

(a)

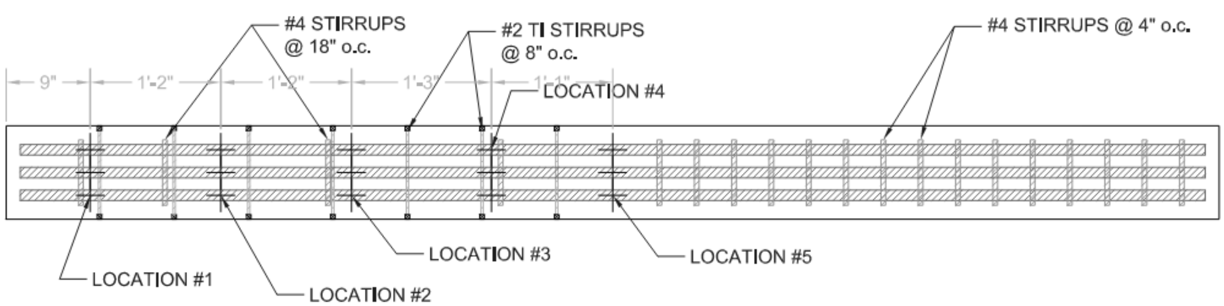

(b)

Figure 19. HCP measurement locations in the shear beam (bottom bars CP), a) Side view); b) Top view).

Results of the tests showed that the applied current densities exceeded the lower bound predicted by polarization scans, consistent with additional resistance within the NSMR-ECSG system. Current levels remained stable during ICCP operation, confirming that TiAB stirrups and ECSG provided effective electrical continuity as seen in Fig. 17a and b. These results are consistent with those observed in the flexural beam as shown in the same figure. Depolarization results, shown in Figures 20 and 21 demonstrated that all of the evaluated reinforcement satisfied the 100 mV criterion. However, spatial variations were observed. Reinforcement located closer to TiAB stirrups exhibited greater polarization, while reinforcement locations beyond the final TiAB stirrup showed smaller potential shifts. This confirms the localized nature of ICCP protection when anodes are discretely spaced.

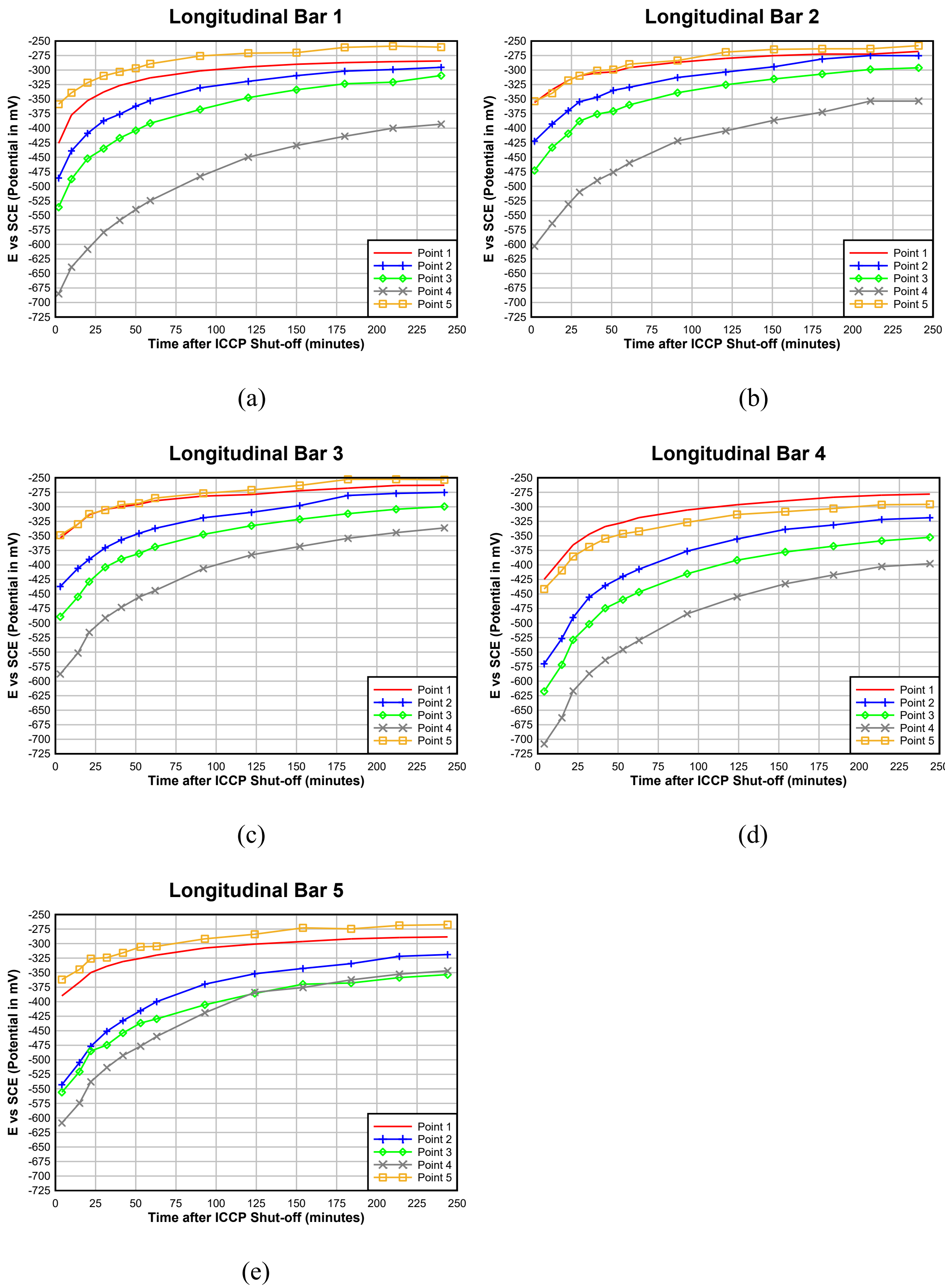

Figure 20. Depolarization of the longitudinal steel rebar in the shear beam after the ICCP current is terminated.

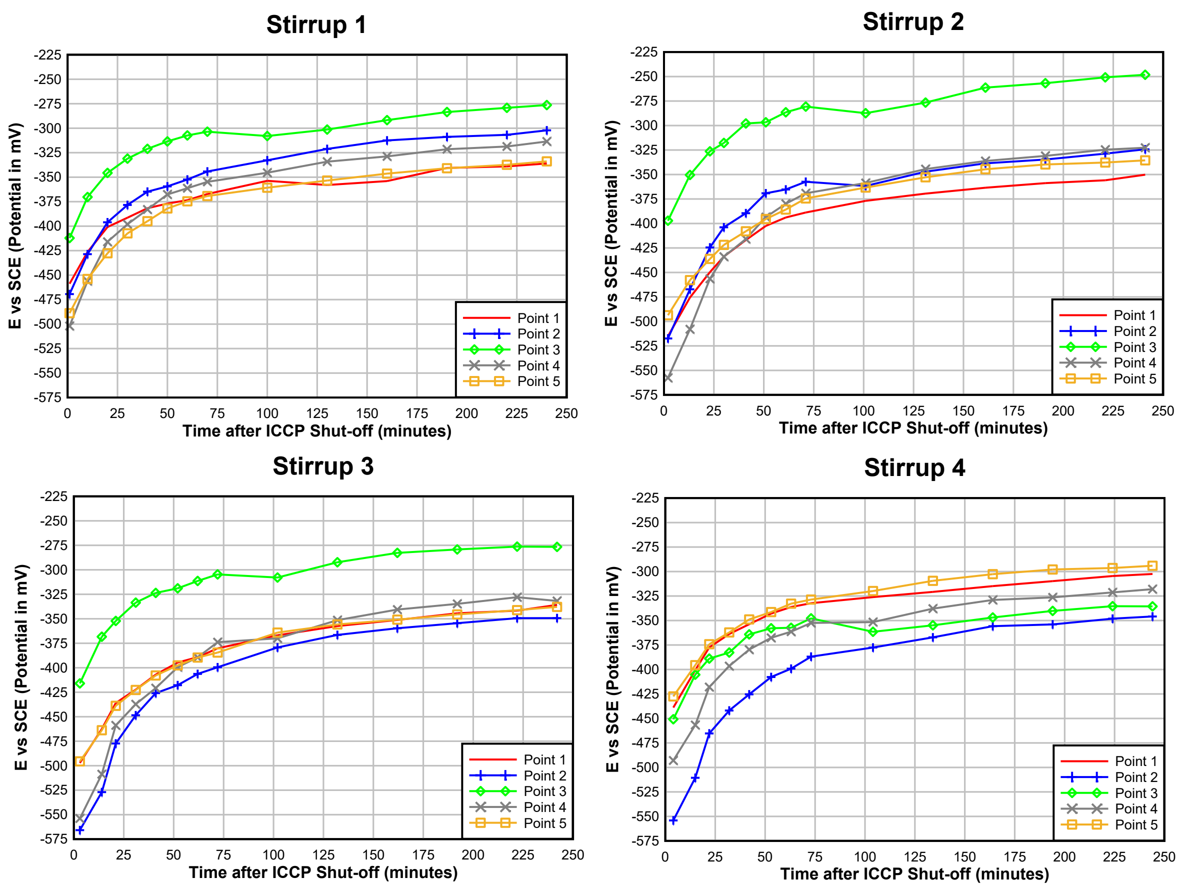

Figure 21: Depolarization of the transverse steel stirrups in the shear beam after the ICCP current is terminated.

Summary of Electrochemical Performance

The electrochemical evaluation demonstrated that TiABs installed using ECSG can function as ICCP anodes. The system exhibits favorable electrical resistivity characteristics, predictable polarization behavior, stable current demand, and compliance with accepted cathodic protection performance criteria. These results establish the electrochemical feasibility of the integrated NSMR-ICCP system and provides a foundation for the structural performance assessments presented subsequently.

STRUCTURAL PERFORMANCE

Structural Performance of the Integrated NSMR-TiAB-ICCP System

The structural performance of the integrated NSMR and ICCP system was evaluated to verify that TiABs, when installed using ECSG, provide reliable bond, effective force transfer, and predictable strength enhancement while remaining compatible with electrochemical operation. The structural assessment included bond (pullout) testing and large-scale beam testing designed to represent common deficiencies in aging reinforced concrete transportation infrastructure.

Bond Strength

Adequate bond between NSMR reinforcement and the concrete substrate is essential to ensure effective force transfer and to mobilize the strength of supplemental reinforcement. Because ECSG replaces conventional epoxy adhesives in the integrated system, its bond performance was evaluated relative to established NSMR requirements To assess bond strength of ECSG, pullout tests were conducted. Concrete blocks were used for the substrate and both ECSG and conventional structural epoxy were used to bond TiABs into the blocks. Since structural epoxy has been used before with these TiABs, epoxy bond tests were used as a control reference. Different sizes of unreinforced concrete blocks were made according to the required development length of the TiABs, l_{dTi}, prescribed in AASHTO NSMT-1 (2020) as:

$$l_{dTi} = \frac{d_{Ti}}{4}\frac{f_{Ti}}{\bar{\mu}_u} \quad \text{(Eqn. 1)}$$

where d_{Ti} is the diameter of the TiAB, f_{Ti} is the yield strength of TiABs, and $\bar{\mu}_u$ is the ultimate average bond strength of TiABs, prescribed as 1 ksi [7 MPa]. Table 7 shows the development length for Class 130 #2 and #5 TiABs.

Table 7: Embedment depths of TiABs in pullout tests.

TiAB Bar Size	d_{Ti} in. (mm)	f_{Ti} ksi (MPa)	$\bar{\mu}_u$ ksi (MPa)	l_{dTi} in. (mm)
#2	0.25 (6)	130 (900)	1.0 (7)	8.1 (207)
#5	0.625 (16)	130 (900)	1.0 (7)	20.3 (516)

To evaluate the bond strength of the ECSG, unreinforced concrete blocks were cast to provide the approximate embedment depth required for development of each TiAB size used in this study (#2 and #5). Additional concrete blocks were cast to test the TiABs at half the required embedment depth in both epoxy and grout. The mean concrete compressive strength of the concrete blocks was 2600 psi [18 MPa] with 2.7% coefficient of variation (COV). The mean ECSG compressive strength was 7550 psi [52 MPa] with 3.0% COV. Three (3) #5 TiABs were placed in grout with full embedment in concrete to a depth of 20.25 in. [496 mm]. For the half-embedment case, six (6) #5 TiABs were tested: three (3) were bonded with epoxy and three (3) were bonded with the conductive grout at depths of 10 in. [254 mm]. The #2 TiABs were placed in concrete blocks with a depth of 8 in. [196 mm] for full embedment and a depth of 4 in. [100 mm] for the half-embedment case. Three (3) replicates of #2 bars were grouted at full embedment, three (3) were grouted at half-embedment, and three (3) were epoxy bonded at half-embedment.

To install the TiABs, holes were hammer-drilled perpendicular to the top surface of the concrete blocks. The holes were drilled all the way through the blocks to allow access for instrumentation on the unloaded end of the bars. The parameters prescribed in AASHTO NSM-1, specifies groove geometry for the placement of TiABs in epoxy to be equal to $1.5D_{Ti}$, where D_{Ti} is the diameter of the TiAB [5]. For the #2 TiABs, $1.5D_{Ti}$ is 3/8 inches [10 mm]. Based on this prescribed geometry and the requirement that bars are centered within the groove, that leaves a 1/16-inch [2 mm] gap between the walls of the groove and the bar. While this geometry is suitable for epoxy, which is more fluid and easier to place with associated small diameter nozzles, the ECSG utilizes 6 mm [0.25 in] carbon fibers to decrease resistivity, and thus the space between the concrete and TiAB is too narrow to ensure adequate placement of the ECSG without the potential to entrap air pockets. For this reason, the groove dimensions were increased from 3/8 in. [10 mm] to ½ in. [13 mm]. The hammer-drilled holes were created with a 1 in. [25 mm] diameter bit for placement of the #5 TiABs, and a ½ in. [13 mm] diameter bit for the #2 TiABs.

The TiABs were cut to length with sufficient extension to permit the bars to be gripped by the test apparatus. Bars were placed such that the tails extended beyond the bottom face of the concrete block about 1 in. [25 mm] so that they could be instrumented to measure slip at the unloaded end of the bar. Fixtures were used to hold the bars perpendicular to the concrete surface as the bonding materials set. To ensure proper placement of the conductive grout in the holes a hand operated grout pump with a custom modified extension nozzle was used to fill the holes. The small diameter holes used for the #2 TiABs were a particular challenge due to the diameter reducer required on the pump hose which restricted grout flow. It is noted that in the actual NSMR application, the materials are not pumped into holes but instead are placed into grooves with trowels, which simplifies installation. Because the purpose of the experiment was to assess bond strength of the grout at the concrete-grout and grout-TiAB interfaces, a steel reaction plate was used at the concrete surface to prevent development of surface spall cones. The hole diameter in the plate was 2 in. [5 cm]. A center-hole ram in-series with a 50 kip [222 kN] capacity hollow-core load cell was placed on the plate. Prestressing chucks were used to grip the bar and the jack was actuated with a manually operated hand-pump. Sensors measured the displacement of the loaded and unload ends of the bars. Post-processing of the displacement measurements was done to remove bending deformations, instrument slip, artifacts, and electrical noise to resolve the motion to axial deformation. All data were collected with a commercially available data acquisition system at a sampling rate of 10 Hz (0.1 second intervals). A schematic and a photograph of the pullout test setup are shown in Fig. 22 (a) and (b), respectively.

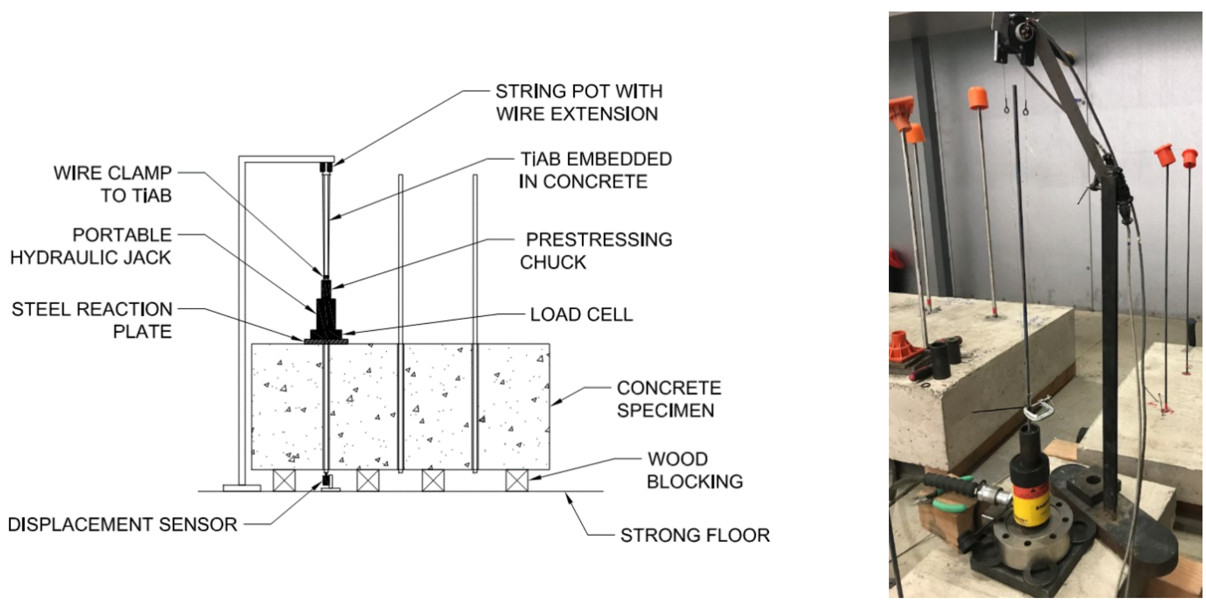

(a) (b)

Figure 22. Pullout test setup (a) schematic, and (b) photograph.

Typical pullout responses observed for the #5 TiABs in different bonding materials and embedment lengths are shown in Fig. 22. For #5 TiABs at full embedment in ECSG, all three (3) specimens achieved the specified minimum yield stress of 130 ksi [900 MPa] and two of the three exhibited ductile yielding. This shows that the ECSG meets the AASTO NSMT-1 bond requirements. For the half embedment in ECSG, all three (3) specimens (one example is shown in Fig. 33) failed due to pullout close to the minimum specified yield stress. Pullout failures exhibited sudden displacement of the unloaded end relative to the concrete. No movement was observed at the unloaded end prior to pullout failure. Based on the exposed surface between the TiAB and ECSG, the interface appeared to be well-bonded due to the presence of the surface pattern deformations in the grout as seen in Fig. 24 and thus failure occurred at the concrete-ECSG interface. All three (3) epoxy bonded TiABs at half embedment achieved the minimum yield stress with ductile yielding and meet AASTO NSMT-1 bond requirements. The average bond strength was computed for those samples exhibiting pullout failure as the peak applied load divided by the bar perimeter and embedment length and are reported in Table 8. The average minimum bond stresses for samples that exhibited ductile yielding were computed as the peak applied load divided by the bar perimeter and embedment length and are also reported in Table 8.

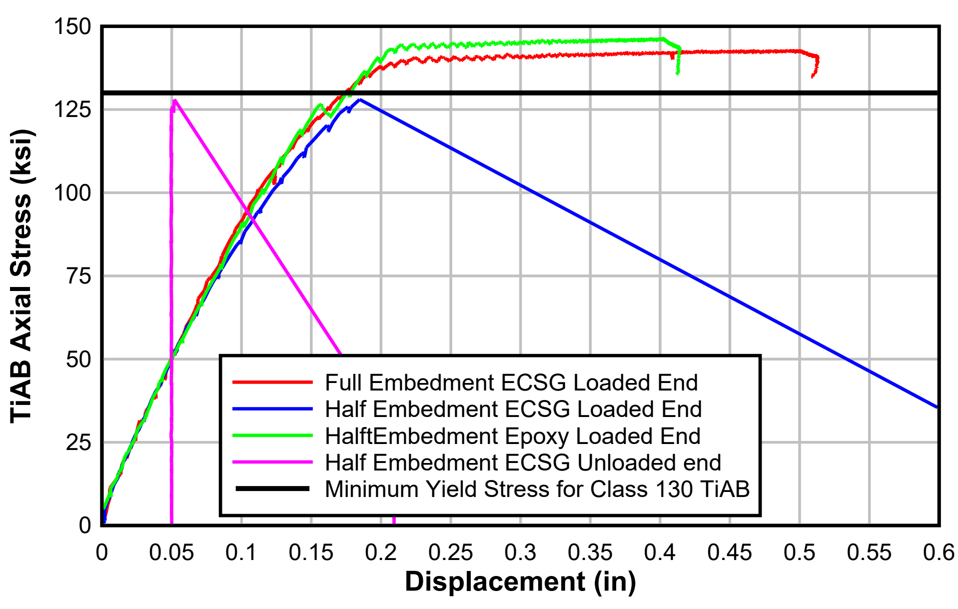

Figure 23. Example pullout test results for #5 TiAB specimens with different embedment and bonding materials.

Figure 24. TiAB pullout failure at concrete-ECSG interface (note how TiAB deformation surface is visible in ECSG).

Typical pullout responses observed for the #2 TiABs in different bonding materials and embedment lengths are shown in Fig. 25. For #2 TiABs at full embedment in ECSG, all three (3) specimens achieved the specified minimum yield stress of 130 ksi [900 MPa] with substantial ductile yielding. This shows that the ECSG meets the AASTO NSMT-1 bond requirements for the #2 bars. For the half embedment in ECSG, all three (3) specimens, shown in Fig. 24, failed due to pullout at widely varying stress levels. The pullout failures are attributed to variability in placement of the ECSG into the small diameter holes. All three (3) epoxy bonded TiABs at half embedment achieved the minimum yield stress with ductile yielding and exceed AASTO NSMT-1 bond requirements. The average bond strength was computed for those samples exhibiting pullout failure as the peak applied load divided by the bar perimeter and embedment length and are reported in Table 8. The average minimum bond stress for samples exhibiting ductile yielding was computed as the peak applied load divided by the bar perimeter and embedment length and are also reported in Table 8.

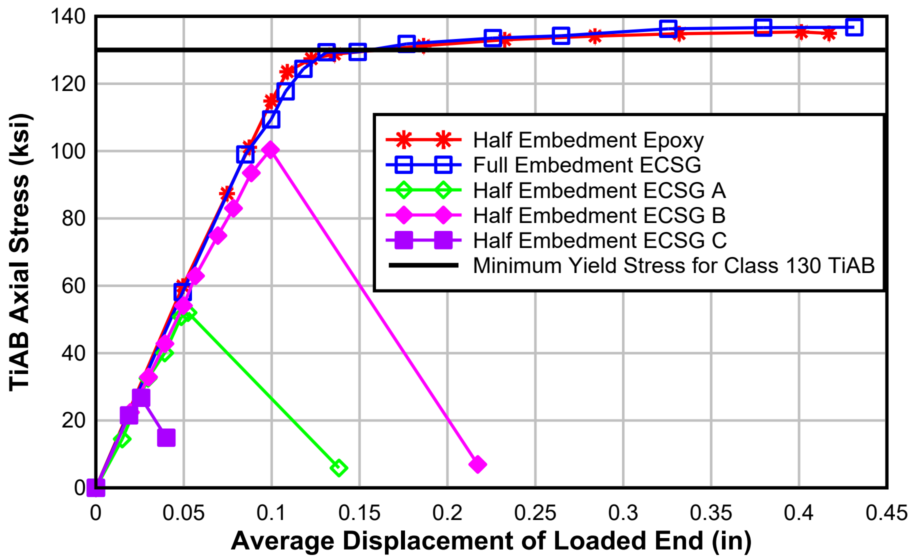

Figure 25. Example pullout test results for #2 TiAB specimens with different embedment and bonding materials.

Table 8: TiAB pullout test results.

Bar Size #	Bonding Material	Embed. Length in (mm)	Hole Diameter in (mm)	Peak Load kips (kN)	Maximum TiAB Stress ksi (MPa)		Average Bond Stress psi (kPa)	
#5	ECSG	20.25 (514)	1.0 (25)	40.6 (181)	135 (932)		567 (3909)	*
				42.9 (191)	143 (986)	Y	599 (4130)	
				43.2 (192)	144 (994)	Y	604 (4164)	
#5	ECSG	10 (254)	1.0 (25)	38.4 (171)	128 (883)		1087 (7495)	*
				35.5 (158)	118 (814)		1003 (6915)	*
				39.6 (176)	132 (908)		1119 (7715)	*
						Average	1070 (7375)	
						St. Dev.	60 (414)	
#5	Epoxy	10 (254)	1.0 (25)	44.3 (197)	148 (1018)	Y	1253 (8639)	
				44.6 (198)	149 (1025)	Y	1262 (8701)	
				44.0 (196)	147 (1010)	Y	1245 (8584)	
#2	ECSG	8 (203)	0.5 (13)	6.6 (29)	135 (930)	Y	528 (3640)	
				6.8 (30)	137 (943)	Y	538 (3709)	
				6.6 (29)	134 (925)	Y	527 (3634)	
#2	ECSG	4 (102)	0.5 (13)	2.6 (12)	52 (359)		411 (2834)	*
				4.9 (22)	100 (692)		783 (5399)	*
				1.3 (6)	27 (184)		210 (1448)	*
						Average	468 (3227)	
						St. Dev.	291 (2006)	
#2	Epoxy	4 (102)	0.5 (13)	6.7 (30)	136 (938)	Y	1062 (7322)	
				6.6 (30)	135 (934)	Y	1057 (7288)	
				6.8 (30)	139 (956)	Y	1084 (7474)	

Y: TiAB achieved minimum specified yield stress.
*: Maximum measured average bond strength.

The observed bond behavior of ECSG-bonded TiABs was comparable to that of epoxy-bonded systems when appropriate embedment lengths were provided. Importantly, bond failures, when they occurred, were governed by separation at the concrete–grout interface rather than at the TiAB–grout interface, indicating strong mechanical interlock between the deformed TiAB surface and the ECSG. These results confirm that ECSG can serve as a structurally adequate bond medium while simultaneously enabling electrical conductivity required for ICCP operation.

Large-Scale Beam Test Program

To evaluate system-level structural performance, the two large-scale reinforced concrete beam specimens were tested under monotonic loading. The flexure-dominated specimen contained insufficient flexural reinforcement with adequate transverse reinforcement to preclude shear failure and the shear-dominated specimen contained minimal transverse reinforcement and sufficient flexural capacity to ensure diagonal-tension failure. In both beams, TiABs were installed as near-surface mounted reinforcement using ECSG and their electrochemical performance within an ICCP system was described previously. This configuration allowed direct evaluation of whether the dual-function installation affected structural response.

Instrumentation and Testing Protocols

A broad array of sensors were deployed to characterize the structural performance of the beam specimens. Strain gauges were bonded to the reinforcing steel and TiABs at selected locations prior to concrete placement. Because the concrete was heavily salted, additional precautions were taken to protect the strain gauges and lead wires from corrosion, and all connection locations were coated with a corrosion-resistant sealant. Prior to testing on the laboratory strong floor, the specimens were instrumented with displacement transducers to measure both global and local deformations.

The displacement transducer layout for the shear specimen is shown in Fig. 26. The flexural specimen was instrumented with displacement transducers only at midspan and over the supports. The strain gauge layouts for the flexural and shear specimens are shown in Figs. 27a and 27b, respectively. Applied load was measured using a load cell mounted to the hydraulic actuator. All data were recorded using a commercially available data acquisition system at a sampling rate of 100 Hz.

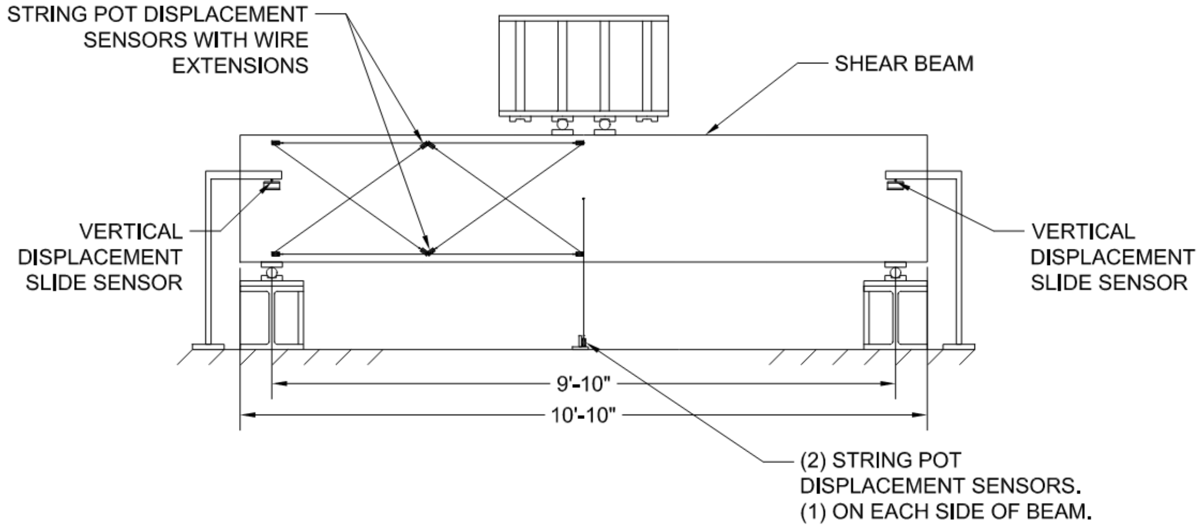

Figure 26. Location of displacement sensors on shear beam specimen.

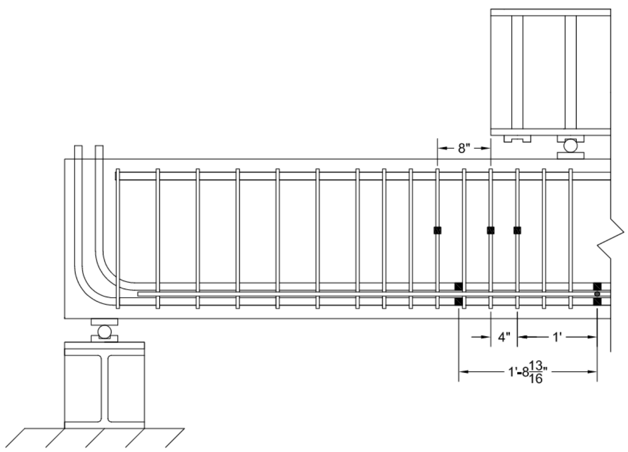

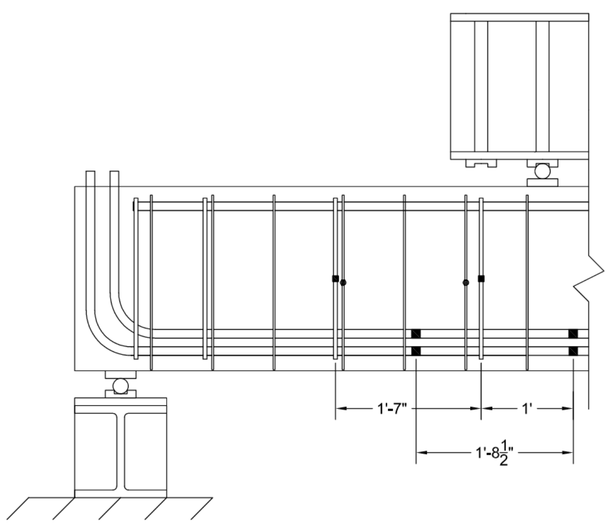

Figure 27. Locations of strain gages on (a) flexural beam specimen and (b) shear beam specimen.

Both beams were tested under four-point bending; however, the test spans differed between the two specimens. The test configurations for the flexural and shear specimens were shown previously in Figs. 7 and 8, respectively. Tests were conducted under displacement control using a servo-hydraulic actuator with 500 kip [2224 kN] capacity. The displacement rate was maintained at 0.001 in./s [25.4 μm/s]. Loading was applied in increments of approximately 25 kip [111 kN], followed by partial unloading of approximately 5 kip [22 kN] to allow for visual inspection of the concrete surface while minimizing creep effects. Crack initiation and propagation were visually observed and marked at each load interval until specimen failure.

Flexural Strength and Behavior

The overall load-midspan deflection response of the flexural specimen is shown in Fig. 28. The flexural specimen exhibited an initial elastic uncracked response followed by elastic cracked behavior as loading progressed. Flexural macrocracks were first observed near midspan at an applied load of 35 kips [156 kN], coinciding with the first appearance of a diagonal crack within the shear span. Diagonal cracking remained limited throughout the test.

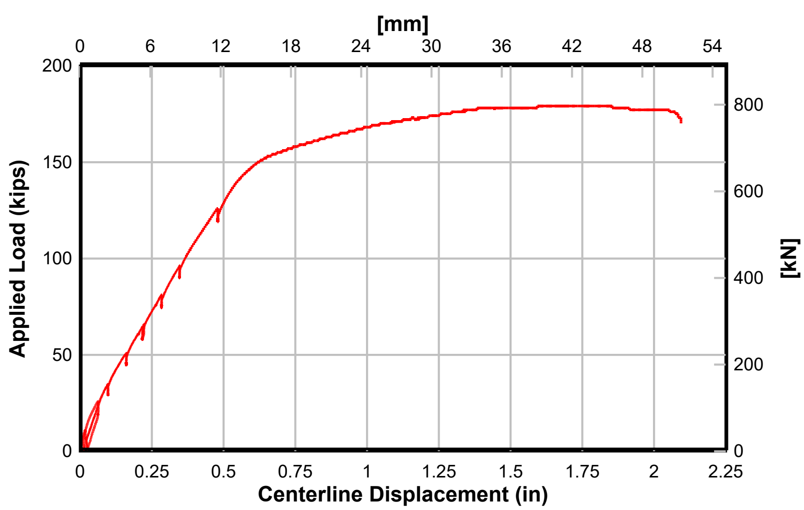

Figure 28. Overall load-midspan deflection response of flexural specimen.

Plastic deformation initiated at a midspan displacement of 0.55 in. [13 mm]. The specimen reached a maximum applied load of 178 kips [792 kN] at a corresponding midspan displacement of 1.59 in. [40.4 mm]. Beyond this point, the specimen experienced a reduction in load-carrying capacity and ultimately failed due to crushing of the compression zone near the loading points at a midspan displacement of 2.09 in. [53.1 mm]. The observed behavior is characteristic of a ductile flexural failure.

Strain measurements from gauges bonded to the embedded reinforcing steel and NSM TiABs in the flexural specimen at midspan are shown in Fig. 29. Comparison of the measured strains in the reinforcing steel and TiABs shows compatible strain behavior well into the plastic range. This demonstrates that the ECSG effectively maintained strain compatibility within the section until about 2 kips [9 kN] from the ultimate load. At that stage, both the bottom steel and TiABs show abrupt strain changes, attributed to spalling and localized debonding. All but one of the instrumented steel stirrups remained elastic throughout the test, consistent with the limited and well-confined diagonal cracking observed within the shear span due to the presence of closely spaced stirrups.

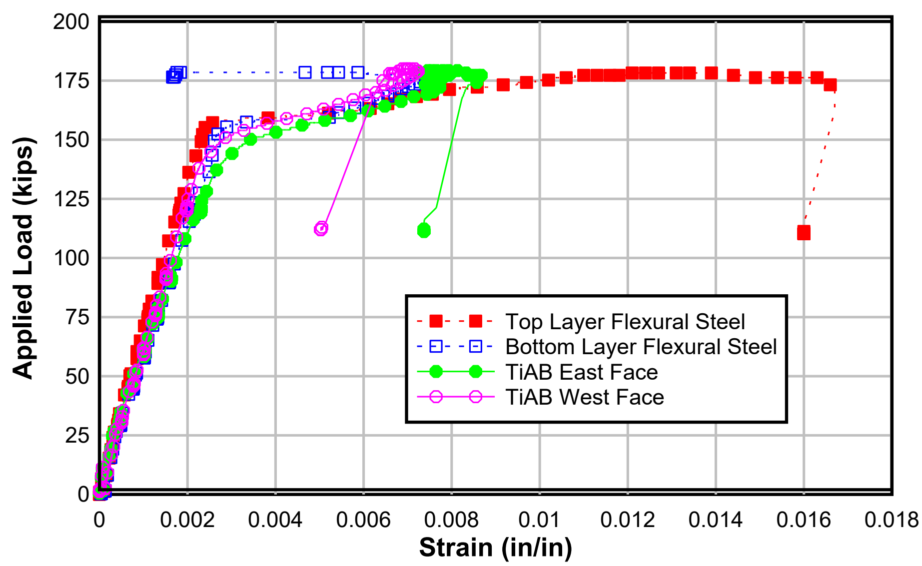

Figure 29: Strains in flexural reinforcing steel and TiABs for flexural specimen.

Shear Strength and Behavior

The overall load-midspan deflection response of the flexural specimen is shown in Figure 30. The shear specimen exhibited an initial elastic uncracked response followed by elastic cracked behavior as loading progressed. Flexural macrocracks were first observed near midspan at an applied load of 35 kips [156 kN]. The first diagonal crack within the shear span occurred at the same load on the unstrengthened half of the specimen and at 50 kips [222 kN] on the TiAB-strengthened half. Diagonal cracks subsequently propagated and widened throughout the test.

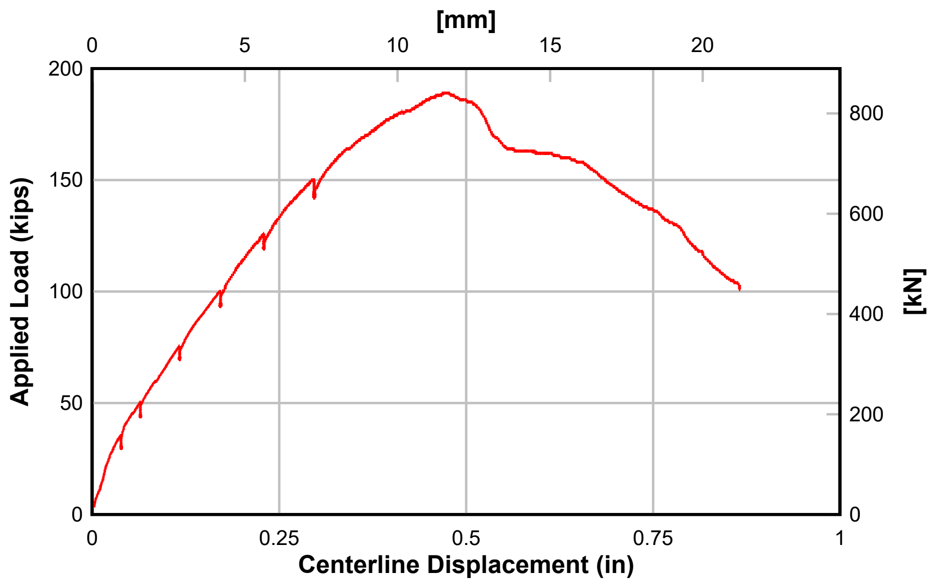

Figure 30. Overall load-midspan deformation response of shear specimen.

Peak load occurred at a midspan displacement of 0.40 in [10 mm]. The specimen reached a maximum applied load of 189 kips [841 kN] at a corresponding midspan displacement of 0.56 in. [14 mm]. Following peak load, the specimen softened and failed due to loss of the compression zone at the loading point. The observed response is characteristic of a nonductile diagonal-tension failure and the specimen condition at failure showed a large amount of distress as shown in Fig. 31.

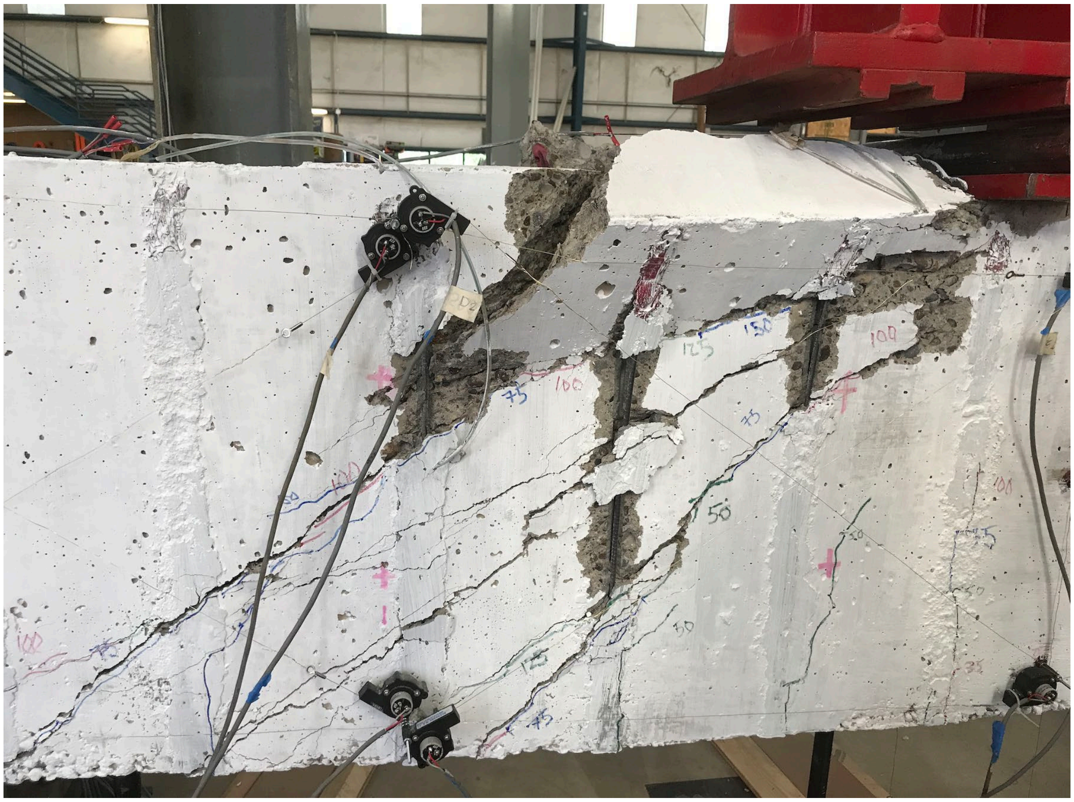

Figure 31. Failure condition for shear specimen.

Strain measurements from the embedded reinforcing steel and NSM TiABs stirrups in the shear specimen are shown in Fig. 32. Measured stirrup strains were influenced by extensive diagonal cracking and associated spalling; however, the TiAB stirrups showed higher strains than similar adjacent steel stirrups. The TiAB stirrup located 23 in. [584 mm] from the loading plate, within the critical region, was seen to have the largest strains and achieved yield. The adjacent steel stirrup also achieved yielding earlier in the loading process at around 85 kips [378 kN]. The relatively short development lengths of the small-diameter bars used for both steel and TiAB stirrups result in sensitivity to location along the span, such that modest differences in the crossing elevation of the diagonal crack relative to the strain gauge location can produce substantial differences in measured strain.

Only limited yielding was observed for the flexural steel as midspan. Here, the bottom layer of flexural reinforcement only marginally reached the yield strain, while the upper layer remained elastic. At the section located within the depth of the section from the edge of the loading plate, flexural reinforcement strains were similar in magnitude to those measured at midspan, indicating increased demand in the flexural steel due to the presence of diagonal cracking. At this location, the upper layer of flexural reinforcement exhibited higher strains than the lower layer, again due to the diagonal cracking.

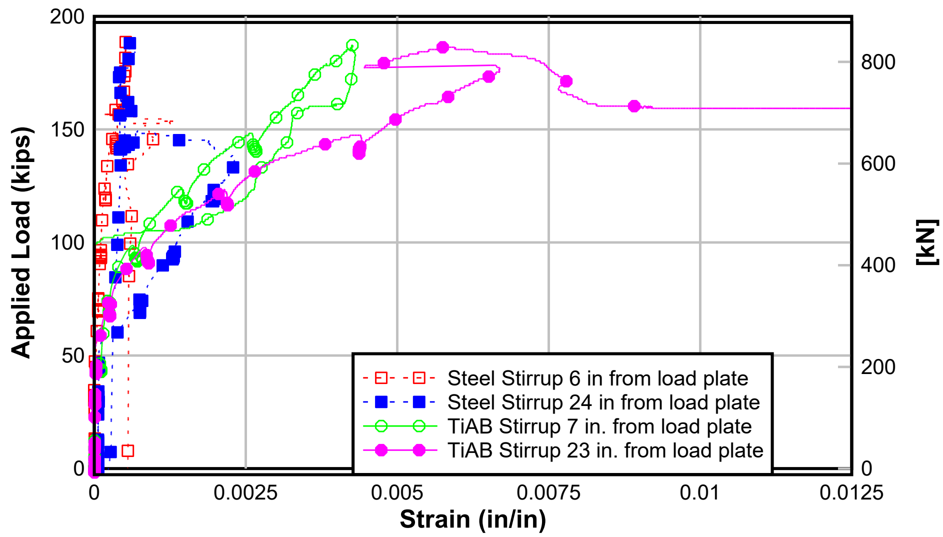

Figure 32. Strains in transverse reinforcing bars for shear specimen.

Comparison of Beam Experimental Results with Analytical Predictions of Strength

Using the as-built section properties, test span dimensions, measured yield stresses of the reinforcing steel and TiABs, and the concrete compressive strength at the time of testing, the strengths of the test specimens were evaluated using several analytical and design methods. The methods considered included ACI 318-25 (2025), AASHTO-LRFD (2020), AASHTO NSMT-1 (2020), and Response-2000 (Bentz, 2000).

The unretrofitted strengths of the specimens were predicted using Response-2000 with the contribution of the TiABs determined by subtracting the expected unretrofitted specimen capacity, adjusted based on the previously observed bias of the analysis method (Higgins et al., 2004), from the experimentally measured strength. For the flexural specimen, the TiABs increased the moment capacity from an expected unretrofitted value of 425 kip-ft [576 kN·m] to 520 kip-ft [704 kN·m], representing a 22% increase. For the shear specimen, the shear capacity increased from an expected unretrofitted value of 69.5 kips [309 kN] to 94.5 kips [420 kN], corresponding to a 36% increase.

Good agreement was observed between predicted and experimentally measured flexural and shear strengths, supporting the assumption of idealized bond behavior for the ECSG adopted in this study. For the shear specimen, the predicted strength was within 3.6% of the experimentally measured capacity, further demonstrating the ability of Response-2000 to capture diagonal-tension behavior, even with the incorporation of novel materials.

Design-based predictions were then developed using ACI and AASHTO methods to estimate nominal strengths. All standard assumptions prescribed in the relevant specifications were applied, including use of an idealized concrete compression zone (Whitney stress block), neglecting concrete tensile strength, strain compatibility with perfect bond between steel, TiABs, and concrete, and elasto-plastic material behavior for both steel and TiABs. The as-built geometry (Figs. 9 to 12) and measured material properties from Table 3 were used in all analyses. Resistance factors were not applied, and the environmental durability factor was omitted for the AASHTO NSMT-1 analyses.

For application of the AASHTO NSMT-1 method to the shear specimen, the shear capacity was determined iteratively by assuming a factored applied shear and using the full shear span of 4.58 ft [1.40 m] to compute the corresponding factored moment. This approach is consistent with a conservative design procedure.

The nominal design strengths were compared with experimental results in Table 9. In all cases, the predicted nominal flexural capacity was conservative relative to the measured strength. For the flexural specimen, the AASHTO NSMT-1 and ACI design methods produced identical nominal moment capacities, as both are based on the same underlying assumptions. Owing to the relatively low concrete strength, the neutral axis depth was predicted to be relatively deep, resulting in elastic TiAB strains at nominal strength. However, the substantial confinement provided by the compression reinforcement and closely spaced stirrups likely permitted ultimate concrete strains exceeding the assumed value of 0.003, thereby increasing section curvature and enabling the TiABs to reach yield, as observed experimentally.

For the shear specimen, the AASHTO NSMT-1 method, based on modified compression field theory, conservatively predicted the shear capacity with a margin of approximately 4%. The ACI shear method, which employs a simplified concrete contribution, slightly overestimated the experimental shear capacity by approximately 1%. Application of resistance factors in design would result in the AASHTO NSMT-1 method producing the lower design strength.For the shear specimen, AASHTO NSMT-1, based on modified compression field theory, conservatively predicted the shear capacity with slight conservatism (4%). Using the ACI method with the simple concrete contribution to shear, the predicted shear strength was only slightly overestimated compared to the experimentally observed strength (1%). The further application of resistance factors in these code methods would result in the AASHTO NSMT-1 method having higher design strength.

Table 9: Comparison between predicted and measured strength.

Method	Flexure Specimen			Shear Specimen		
	Moment Capacity kip-ft	(kN-m)	Measured/Predicted	Shear Capacity kip	(kN)	Measured/Predicted
Experiment	520	(704)	-	94.5	(420)	-
ACI 318	470	(637)	1.11	95.4	(424)	0.99
AASHTO NSMT-1	470	(637)	1.11	91.3	(406)	1.04
Response-2000	501	(679)	1.04	91.2	(406)	1.04

Overall, the analytical and design-based predictions demonstrated good agreement with the experimentally measured behavior of both specimens, supporting the use of conventional analysis assumptions for evaluating NSM TiAB systems embedded in ECSG. Response-2000 accurately captured both flexural and diagonal-tension behavior, providing confidence in the assumption of idealized bond between the TiABs and concrete for the configurations studied. Design methods from ACI 318 and AASHTO NSMT-1 produced conservative nominal strength estimates, particularly for flexure, where confinement effects and strain redistribution enabled the TiABs to reach yield beyond code-based assumptions. For shear, the AASHTO NSMT-1 method provided a slightly conservative prediction, while the ACI approach slightly overestimated strength, with both methods producing reasonable agreement with experimental results. Collectively, these findings indicate that existing analytical and design frameworks can be extended to the NSM-TiAB-ICCP system with appropriate consideration of material behavior, confinement, and detailing.

Summary of Structural Performance

The structural evaluation demonstrates that TiABs installed using ECSG provide effective bond, predictable load transfer, and significant enhancement of flexural and shear capacity when used as near-surface mounted reinforcement. The integrated NSMR-TiAB-ICCP system produced conventional failure modes with strengths that are predictable with conventional engineering methods, while enabling simultaneous corrosion protection.

CONCLUSIONS AND FUTURE WORK

This study evaluated an integrated near-surface mounted reinforcement (NSMR) and impressed current cathodic protection (ICCP) system in which titanium alloy bars (TiABs) serve as both structural strengthening elements and distributed anodes. Small-scale prism testing established electrochemical behavior and current demand, while pullout tests and large-scale flexural and shear beam specimens evaluated structural performance.

The experimental results demonstrated that TiABs installed in a specially developed electrically conductive structural grout (ECSG) could simultaneously deliver structural strengthening and effective cathodic protection without adverse interactions between mechanical and electrochemical functions over the relatively short duration of testing.

Based on the experimental results, the following conclusions are presented:

- Dual-function feasibility was demonstrated**.** TiABs functioned as both load-carrying reinforcement and ICCP anodes within the same installation.
- Cathodic protection criteria were satisfied. All tested configurations met the 100 mV depolarization criterion.
- ECSG enabled system integration. The grout provided both adequate bond and sufficient electrical conductivity to support ICCP operation.
- Structural performance was preserved. Strengthening effectiveness, bond behavior, overall response, and failure modes were consistent with conventional NSMR behavior and predictable with conventional design methods.
- ICCP current demand somewhat exceeded surface-based polarization predictions. Higher applied current densities were required due to distributed system resistance within the NSMR-TiAB-ECSG configuration. It is anticipated that MMO coated TiABs could reduce demands.
- No short-term electrochemical instability was observed. Potentials remained stable and above hydrogen evolution limits during testing.
- Spatial protection depended on anode proximity. Reinforcement closer to TiAB elements exhibited greater polarization, particularly in transverse configurations.

- Results are limited to short-duration laboratory conditions. Long-term durability and field performance remain unverified.

These findings established the technical and practical feasibility of the proposed NSMR-TiAB-ICCP system and identify additional development needs prior to field deployment as detailed below.

Future Work

The present study was limited to controlled laboratory testing conducted over short ICCP durations. In practice, ICCP systems are expected to operate for decades under variable environmental and loading conditions. While the experimental results establish the technical and practical feasibility, additional research is required to advance the integrated NSMR-TiAB-ICCP system toward implementation.

A primary area of future investigation is long-term electrochemical durability. Sustained anodic operation of TiABs must be evaluated under extended current application to quantify anode stability, current efficiency, and potential consumption mechanisms. Development and evaluation of MMO coated TiABs may improve electrochemical performance and reduce anode demand (ISO 2018). In addition, the long-term evolution of the TiAB-ECSG interface requires study, including potential changes in interfacial chemistry that could influence electrical continuity and polarization behavior.

The long-term performance of the ECSG requires further investigation. Future work should examine the stability of grout resistivity under sustained current flow, potential chemical evolution within the grout matrix, and the effects of electrochemical exposure on bond durability between the TiAB and surrounding concrete.

Structural-electrochemical interaction must also be assessed beyond short-duration, monotonic laboratory loading. The influence of fatigue loading, cyclic mechanical demands, and environmental exposure on concurrent ICCP operation remains unknown. Long-term bond retention and possible coupling effects between mechanical and electrochemical performance should be evaluated to ensure durability under long-term service conditions.

Further refinement of the anode system is warranted. Optimization of TiAB spacing to improve current distribution and protection uniformity should be investigated. Development of

MMO-coated TiABs specifically engineered for dual structural and electrochemical functionality may enhance performance and extend service life (Krishnan, et al., 2025).

Field validation represents a necessary next step. Pilot installations on in-service transportation structures are needed to evaluate constructability, electrical connectivity, monitoring requirements, and long-term depolarization response under realistic environmental conditions. These field demonstrations should inform design, inspection, and maintenance protocols as well as practical implementation considerations.

Finally, formal design and construction guidance must be developed to support adoption. This includes procedures for selecting operating current, detailing durable electrical connections, and integrating the dual-function system into established NSMR and ICCP design frameworks.

DATA AVAILABILITY STATEMENT

All electrochemical and structural response data that support the findings of this study are in the Zenodo Data Share repository with the identifier https://zenodo.org/records/18735817

REFERENCES

ACI Committee 318, 2025. Building code requirements for structural concrete (ACI 318-25). Farmington Hills, MI: American Concrete Institute.

ACI Committee 440, 2024. Guide for the design and construction of externally bonded FRP systems for strengthening concrete structures (ACI 440.2R-24). Farmington Hills, MI: American Concrete Institute.

ACI 222, 2019. Guide to protection of reinforcing steel in concrete against corrosion (ACI 222-19). Farmington Hills, MI: American Concrete Institute.

Adkins, J., 2025. Personal communication, 28 August.

American Association of State Highway and Transportation Officials (AASHTO), 2020. Guide for design and construction of near-surface mounted titanium alloy bars for strengthening concrete structures (NSMT-1). Washington, DC: AASHTO.

American Association of State Highway and Transportation Officials (AASHTO), 2024. AASHTO LRFD bridge design specifications. 10th ed. Washington, DC: AASHTO.

ASTM International, 2015. Standard test method for corrosion potentials of uncoated reinforcing steel in concrete (ASTM C876-15). West Conshohocken, PA: ASTM International.

ASTM International, 2016. Standard test method for compressive strength of hydraulic cement mortars (ASTM C109/C109M-16a). West Conshohocken, PA: ASTM International.

ASTM International, 2019. Standard test method for bulk electrical resistivity or bulk conductivity of concrete (ASTM C1876-19). West Conshohocken, PA: ASTM International.

ASTM International, 2024. Standard specification for titanium alloy bars for near surface mounts in civil structures (ASTM B1009-24). West Conshohocken, PA: ASTM International.

Bahekar, P.V. and Gadve, S.S., 2017. Impressed current cathodic protection of rebar in concrete using carbon FRP laminate. Construction and Building Materials, 156, pp.242–251.

Bentz, E.C., 2000. Sectional analysis of reinforced concrete members. PhD dissertation. University of Toronto.

Byrne, A., Holmes, N. and Norton, B., 2016. State-of-the-art review of cathodic protection for reinforced concrete structures. Magazine of Concrete Research, 68(13), pp.664–677.

DNV, 2011. Recommended practice: Cathodic protection design (DNV-RP-B401). Høvik, Norway: DNV.

Funahashi, M., 2013. What you need to know about MMO coated metal anodes. In: NACE International Corrosion Conference, Paper No. 2107. Houston, TX: NACE International.

Glass, G., 1999. Technical note: The 100-mV potential decay cathodic protection criterion. Corrosion, 55(3), pp.286–290.

Higgins, C., Amneus, D. and Barker, L., 2015. Methods for strengthening reinforced concrete bridge girders containing poorly detailed flexural steel using near-surface mounted metallics. Report No. FHWA-OR-RD-16-02. Salem, OR: Oregon Department of Transportation.

Higgins, C., Amneus, D. and Barker, L., 2017. Shear and flexural strengthening of reinforced concrete beams with titanium alloy bars. In: Proceedings of the 2nd World Congress on Civil, Structural, and Environmental Engineering (CSEE'17), Barcelona, Spain.

Higgins, C., Miller, T.H., Rosowsky, D.V., Yim, S.C., Potisuk, T., Daniels, T.K., Nicholas, B.S., Robelo, M.J., Lee, A.-Y. and Forrest, R.W., 2004. Assessment methodology for diagonally cracked reinforced concrete deck girders. Report No. FHWA-OR-RD-05-04; SPR 350. Salem, OR: Oregon Department of Transportation.

International Organization for Standardization (ISO)**,** 2018**.** Accelerated life test method of mixed metal oxide anodes for cathodic protection — Part 1: Application in concrete**:** ISO standard..

Jones, D.A., 1996. Principles and prevention of corrosion. 2nd ed. Upper Saddle River, NJ: Prentice-Hall.

Knudtsen, J. and Higgins, C., 2017. Application of titanium alloy bars for strengthening reinforced concrete bridge girders (Part A: Shear). Report No. FHWA-OR-RD-18-01; SPR 775. Salem, OR: Oregon Department of Transportation.

Krishnan, N., Higgins, C. and Isgor, O.B., 2025. Cathodic protection of reinforced concrete infrastructure using MMO-coated titanium alloy bars. In: Durability and corrosion control for C3 structures, Chicago, IL. https://doi.org/10.5703/1288284318036

NACE International, 2000. Impressed current cathodic protection of reinforcing steel in atmospherically exposed concrete structures (SP0290-00). Houston, TX: NACE International.

NACE International, 2016. Testing of embeddable impressed current anodes for use in cathodic protection of atmospherically exposed steel-reinforced concrete (TM0294-2016). Houston, TX: NACE International.

Parvin, A. and Shah, T.S., 2016. Fiber reinforced polymer strengthening of structures by near-surface mounting method. Polymers, 8(8).

Sassani, A. et al., 2017. Influence of mix design variables on engineering properties of carbon fiber-modified electrically conductive concrete. Construction and Building Materials, 152, pp.168–181.

Segan, E.G., Bukowski, J. and Kuma, A., 1982. Titanium anodes in cathodic protection. Report CERL-TR-M-303. Champaign, IL: U.S. Army Construction Engineering Research Laboratory.

Su, M., Wei, L., Zhu, J.-H., Ueda, T., Guo, G. and Xing, F., 2019. Combined impressed current cathodic protection and structural strengthening for corrosion-prone concrete structures. Journal of Composites for Construction, 23(4), 04019021

Sun, M. et al., 2011. Deicing concrete pavement containing carbon black/carbon fiber conductive lightweight concrete composites. In: ICTIS 2011, pp.662–668.

Vavra, E. and Higgins, C., 2017. Application of titanium alloy bars for strengthening reinforced concrete bridge girders (Part B: Flexure). Report No. FHWA-OR-RD-18-03; SPR 775. Salem, OR: Oregon Department of Transportation.